NORTHWESTERN UNIVERSITY

Numerical and Experimental Studies of the Dynamics of Diffusion Flame
Sheets

A DISSERTATION

SUBMITTED TO THE GRADUATE SCHOOL

IN PARTIAL FULFILLMENT OF THE REQUIREMENTS

for the degree

DOCTOR OF PHILOSOPHY

Field of Mechanical Engineering

By

Jocelyn Elaine Renner

EVANSTON, ILLINOIS

June 2008

ABSTRACT

Numerical and Experimental Studies of the Dynamics of Diffusion Flame Sheets

Jocelyn Elaine Renner

A comprehension of the complex dynamics of gaseous combustion requires an understanding of the underlying fundamentals. In this dissertation, I examine planar diffusion flames from both an experimental and numerical perspective.

In the first part of this thesis, I study the extinction of unstrained, planar counter-diffusion flames. The theoretical model describing these flames was previously realized from experiments using the Porous Plug Counter-Diffusion (PPCD) burner. Using this burner, I conducted extinction experiments to determine the limiting extinction curves for propane-oxygen and methane-oxygen flames. The effects of burner configuration on extinction concentration are explored, comparisons between propane and methane are made, and the dependence of extinction concentration on mass flux is examined. In addition to the experimental work, the system was numerically modeled to compare the experimental work to model predictions. Also, using numerical simulations, it is shown that a simple chemistry model captures the essential behavior of the system as well as the more complex detailed chemistry model. Finally, the unstable behavior that was observed

during the experiments is documented with comments as to the severity, types, and onsets of such behavior.

In the second part of this thesis, I numerically simulate the effects of Lewis number on the propagation of circular extinction zones (flame holes). Analyzing the data from the numerical simulations leads to the discovery of a scaling law $v = ar^{-b}$ for the dependence of the hole collapse speed on the hole radius at any phase during the re-ignition (hole collapse) event on the flame sheet. Further observation shows that b depends solely on the dimensionless strain rate and is independent of the Lewis number. Also, it is found that decreasing the Lewis number increases the critical radius (*i.e.* the largest size of the hole that results in a re-ignition of the flame) for a given strain rate and that the scaling exponent of the critical radii with respect to strain rates is independent of the Lewis number. A better understanding of the effects of the Lewis number helps bridge the gap between analytic work where unity Lewis numbers are presupposed in many cases and the dynamics observed through experimentation. This leads to more accurate models of turbulent combustion and flame extinction. An improved understanding of colliding planar flames guides the more complicated problem of flame hole collapse and turbulence as well as having practical applications to various situations, such as in engine design.

Acknowledgements

No one walks alone through the world; therefore, I have many people to thank. Mom and Dad, I can never express in words how much you have given me. Without your love and support, none of this would have been possible. Your encouragement always helped me when I thought there was no end in sight. You will always be the wind beneath my wings. To my brother, Adam, thank you for always tolerating my crazy ideas. I love you so much! You are the best brother a girl could have. Nana, your quiet ways, gentle support, and constant love have always inspired me.

Benjamin, my love, you were always there to brighten my day. I literally could not have done this without you. I look forward to a lifetime with you!

Thanks to Prof. Sandip Ghosal for believing in me, even when I sometimes did not. Prof. Moshe Matalon, I truly appreciate all the guidance, advice, support, and countless explanations. Also, thank you for facilitating my internship at Colorado School of Mines. Prof. Paul Papas, Micah Jakulewicz, and the friends and colleagues at Colorado School of Mines will always have my gratitude for a successful and incredible visit. A huge thanks to Prof. Siavash Sohrab and Prof. Vladimir Volpert for their advice and time serving on my committee. Their insightful comments helped refine this thesis.

Scott Carpenter, thank you so much for teaching me the importance of fundamentals. You will always be my hero.

Thanks to the many friends and family who have been there and cheered me along the way. To Matt for providing inspiration, to Ashlie and Dave for your friendship, and to my officemates for their support.

Table of Contents

List of Tables

List of Figures

CHAPTER 1

Introduction

The phenomena of fire has fascinated humans throughout history–from cooking fires in primitive villages to rockets in the space age. Yet, only in the last one hundred years has humanity started to have an understanding of the mechanisms underlying this essential process. Many different aspects of combustion have been studied through the past century including combustion of solid materials, liquid sprays, and gaseous mixtures. We turn our attention to the third because of the wide range of applications and the richness of the dynamics. The complexity of the chemical reactions, coupled with the difficulties of understanding the underlying fluid mechanics, make the challenge of fully understanding turbulence in combustion a daunting task; however, some insight can be reached by studying simplified models of combustion under limiting cases. Through these studies, questions such as when will a gas ignite, how does the flame propagate, and under what circumstances will the flame be extinguished are posed to gain deeper insight into the mechanisms that govern combustion and the conditions necessary for it.

Gaseous combustion can be roughly separated into two different regimes: the slow burning regime, called deflagrations, are those typically associated with flames such as those found in burners and the fast burning regime, called detonations, that are associated with explosions. Here, only the slow burning flames (those with a propagation speed much less than the speed of sound) will be considered. Within this grouping, flames are generally categorized into premixed flames and non-premixed flames (diffusion flames).

In Chapter 2, I will present a look at some of the relevant work in the field, explain the experimental burners that have been used, and explain the importance of the Lewis number, a parameter that will be explored during this study. This understanding of the history of combustion will provide the background for the models and experiments to be presented.

Chapter 3 discusses the experimental and numerical work conducted at Colorado School of Mines under the guidance of Prof. Paul Papas. This work was implemented with the porous plug counter diffusion (PPCD) burner, a new apparatus designed to study flames in uniform flows with very low strain rate. Experimental and numerical work on the extinction limits for propane and methane in this burner (and hence in the limiting case of zero strain rate) are presented. For both experiments and simulations, the effects of burner configuration on extinction concentration is examined showing that the flames extinguish at different concentration depending on whether fuel or oxidizer is flowing and which side of the extinction curve is under investigation (fuel lean or fuel rich). Comparisons between propane and methane show that propane is a more stable gas that allow lower concentrations at extinction. The dependence of extinction on concentration on mass flux is carefully analyzed showing that there are certain regions where the mass flux must be reduced or increased to create burning, and that the extinction curve is highly sensitive to the mass flux used to determine the extinction concentration. We also are able to bridge the gap between analytical models of unstrained counter diffusion flows that presume only simple chemistry and the numerical multicomponent chemical models by using a simple, numerical, one-component chemical model and showing how this captures the same dynamics as that of the more complex chemistry, validating the

comparisons between the analytic models and the numeric models. Finally, the unstable (non-linear) behavior of various extinction limits and a description of the observed instabilities is presented with explanations as to the onset of the oscillations, how they develop, their severity and how they differ between fuel types.

In Chapter 4 I extend the work of Ghosal and Vervisch [1] and Lu and Ghosal [2, 3] to numerically consider the effects of Lewis number on a two dimensional colliding flame model. I am able to fit the velocity of the edge of the flame near collapse to a polynomial expression and determine that the coefficient is dependent on Lewis number while the exponent is dependent on strain rate. Also, a study of the effects of Lewis number on critical radius is examined showing how Lewis number increases the critical radius within a given strain rate and that all critical radii scale between strain rates in the same fashion.

An improved understanding of colliding planar flames provides insight into more complicated problems such as flame hole collapse and turbulence as well as having very practical applications to engine design (see for example the work conducted by Carrier, *et al.* [4, 5, 6, 7]). This experimental work provides a framework to study analytic models of flame dynamics and multistep chemistry and allows for verification of experimentally determined parameters. It also opens a new dimension in looking at oscillatory behavior in the extinction regimes. Finally, having a better understanding of the effects of the Lewis number helps bridge the gap between analytic work (where unity Lewis numbers are presupposed in many cases) and the dynamics observed through experimentation, and could lead to greater understanding of turbulent combustion and flame extinction. While the work proposed here will contribute to the general understanding of combustion and flame dynamics, the methods and mathematical models described can also be applied

to other fields such as chemistry, material science, and fluid dynamics. In addition to combustion, they can be used to study problems related to bubbles, crystals, or corrosion [8].

CHAPTER 2

Background

Many summaries of the literature on gaseous planar flames are available (see for example [**9, 10, 11, 12**]). Only a brief examination is attempted here. This chapter will encompass some of the background that has led to the current work.

While alchemists and scientists throughout the ages have studied fire in various forms, Mallard and Le Chatelier were the first to study how combustion fronts propagated as they attempted to understand how fires in mines traveled [**13**], and many others have attempted to solve the problems involving combustion in various forms [**9**]. From detonations (explosions) to deflagrations (burning flames), these problems are vast in scope and difficulty. Due to the highly non-linear nature of the equations governing both the fluid dynamics and the heat and mass transfer, no analytic solution is possible to the more complex models. Different simplifications resulted in many different approximations for flame speed and models for flame propagation. Taffanel, Jouguet, Nusselt, Daniell, Lewis and von Elbe, and others developed solutions to simplified models or experimentally determined expressions for flame propagation. The precursors to modern asymptotic methods of studying planar flame speeds came from Zeldovich and Frank-Kamenetskii who developed a model for flame propagation in the limit of large activation energy (represented by a parameter now known as the Zeldovich parameter (β)). Teffanell, Zeldovich and Frank-Kamenetskii all considered an Arrhenius model reaction rate. The latter two developed a model to consider concentration and temperature in the reaction zone [**10**].

Gaseous flames may be classified in two broad types: premixed flames and non-premixed (diffusion) flames. Premixed flames are formed when a flame front propagates through a homogeneous mixture of fuel and oxidizer. If the fluid flow in the gas is laminar then the resulting flame is known as a laminar premixed flame. Premixed flame fronts can be steady (such as in a Bunsen burner) or they may take the form of a traveling front. Diffusion (non-premixed) flames occur when fuel and oxidizer are introduced from different sides of the flame front. Common examples include candles, some gas stoves, and counterflow burners (more explanation on this later).

2.1. Premixed Flames

Premixed flames have been a subject of active research because of its direct applications and because their essential properties can be described by relatively simple mathematical models. These flames will be briefly discussed as some theories are essential to understanding their more complex cousins, non-premixed flames.

In his 1965 work, Williams [14] presented a summary of the research on premixed laminar flames, describing the history behind the study, experiments, and current theories. He summarized a phenomenological analysis and the mathematical theory behind the deflagration waves. Since then his model has been used by many others. An important aspect of the derivation he presents is the cold boundary difficulty where the boundary conditions suggested cannot be met in terms of the actual problem, *i.e.* the problem is ill posed. One possible correction is to simply set the reaction rate to zero when the temperature is less than some ignition temperature. Some approximation techniques, including Von Kármán's solution and Zeldovich's are presented.

Zeldovich and Frank-Kamenetskii's asymptotic approach to studying flame propagation paved the way for the application of the field of asymptotics to combustion that developed in the 1950's and 1960's as well as the theory of large activation energy asymptotics (now simply known as AEA). Friedman and Burke presented a leading order expansion for the case of unity Lewis number[1] and the numerical work to examine the solution. Bush and Fendell continued their work and presented a two term asymptotic solution for temperature and concentration in the limit of high activation energy, considering general Lewis numbers [15].

Following the development of analytic solutions for an infinite domain came the development of solutions for quenching of flames. Engine design was one major motivation for studying flame collision with walls and flame quenching (see for example: [16, 6, 7]). Kurkov and Mirsky studied laminar flame extinction on a cold wall and developed an asymptotic solution [16]. Part of the fuel remains unreacted in the cold wall problem as the flame is quenched away from the wall. Kurkov and Mirsky studied how the amount of unreacted fuel depends on the Lewis number and gave a lower limit for the amount of unreacted fuel. Carrier, Bush, Fendell and others [4, 5, 6, 7] conducted in depth studies of flames interacting with adiabatic (non-reacting) walls and with cold walls in an effort to improve engine design. Their work on adiabatic walls showed that the flames do not quench before the wall, but the flame speed actually increases as the flame approaches the wall and there is complete combustion of the deficient species. They developed a similarity solution for the unity Lewis number case of a laminar flame with an adiabatic boundary condition and studied it numerically, later extending their work to include side

---

[1] The Lewis number is the ratio of the thermal diffusivity of the mixture to the mass diffusivity of the deficient reactant

walls [**5, 4, 7**]. Bush, *et al.* discuss the engineering ramifications of their work, including the potential for ceramic (close to adiabatic) caps for engines versus caps held at a uniform temperature. Interestingly, they note that the materials could not withstand the temperature fluctuations at the wall caused by reaction with a pure adiabatic wall; however, this produced more efficient burning and less loss of heat to the surroundings. [**6**].

Other works extended the one dimensional model to include pressure disturbances and their effect on flame behavior, constant volume flame propagation and oscillations in flames [**17, 18**]. Buckmaster examined two dimensional premixed flames, including work on quenching due to heat loss and quenching due to shear behind a wire. He showed how the flame speed depends on the heat lost: small heat losses cause the flame speed to increase and large heat losses cause the flame speed to decrease. Large shear gradients quench most flames (note they did find a small band of Lewis numbers for which quenching does not occur) [**19**]. Recently, models including a higher number of reactants have been introduced including the work by Matalon, Cui, and Bechtold where they presented a two-reactant scheme to study the effects of varying the effective Lewis number. They considered the velocity, pressure, and vorticity generated by the flames and studied several physical examples of flames such as a Bunsen burner and flames stabilized by a stagnation point [**20**].

The mathematics behind premixed flames also has applications to other fields. Duda and Vrentas [**8**] developed a method of solving moving boundary problems in diffusion controlled systems using perturbation methods similar to those used in combustion, and they suggested applications of their work include bubble dissolution, growth of crystals in

liquids, corrosion of metals, and sorption of penetrants by polymers. In a related work, Huang and Shih [21] studied liquid freezing. Many of the same techniques used in Huang & Shih and Duda & Vrentas, such as using coordinates attached to the moving boundary, are used in studying planar flame deflagration.

2.2. Diffusion Flames

Diffusion flames generally occur when there is a separation between the fuel and the oxidizer (such as methane gathering in the ceiling of a mine with fresh air below) with a flame at the interface between the two. Partial premixing also can lead to diffusion like flames where characteristics of both premixed flames and non-premixed flames are observed [12]. Tribrachial flames (also known as triple flames), which combine aspects of partial premixing and diffusion flames, occur in a variety of situations, from flame spread over liquid fuels to strained jets [22]. They are comprised of a fuel rich premixed branch and an oxidizer rich premixed branch with a diffusion flame between. One common manifestation of this phenomena is an edge flame that develops where the flame sheet ends either due to quenching (such as in the case of a flame hole or a disk) or due to stabilization off of a burner, splitter, or heat sink (see Figure 2.1). A flame sheet that develops a hole, usually due to quenching can be thought of as a ring of edge flames, as can its counterpart: a flame disk that develops when a patch of burning material is surrounded by unignited gas. Understanding the dynamics of flame holes and flame disks is important to gaining more insight into the behavior of flame sheets and turbulent combustion [23]. A brief background on previous research into diffusion flames, edge flames, and holes and

disks in flame sheets, including a review of analytical, numerical and experimental work, is presented in Section 2.2.1.
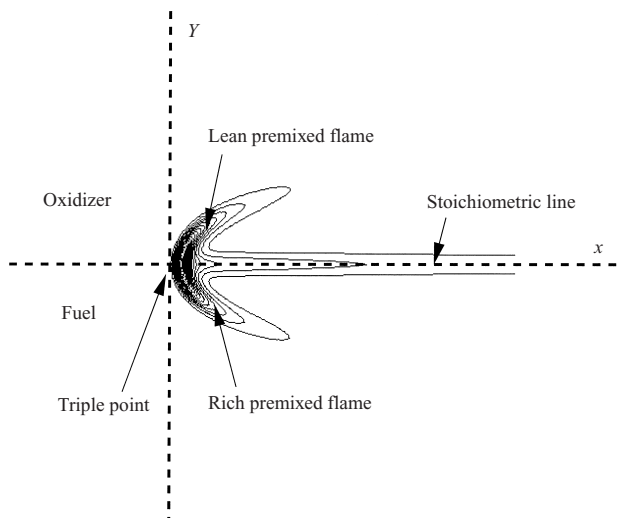
Figure 2.1. Diagram of an edge flame. Fuel and oxidizer are separate, as for diffusion flames. As the flame propagates into the region a lean premixed flame and a rich premixed flame are observed on either side of a diffusion flame. Numerical calculation from Ruetsch, *et al.* [**24**] reproduced from Ghosal and Vervisch [**1**]

2.2.1. Planar Two Dimensional Diffusion Flames

Burke and Schumann [**25**] coined the phrase "diffusion flame" in their preliminary work on non-premixed flames. Their experimental work, as discussed in the previous section, supplemented their theoretical predictions. Their model was a one dimensional, constant coefficient, steady flame model where they assume that the flame was confined to a thin region they referred to as the flame front. The reduced equations they developed were those governing the diffusion of a single gas with boundary conditions of constant concentration at infinity and a boundary condition at the flame front. They considered

both spherical burners and flat flames, giving flame profiles for both cases. They showed how varying different parameters such as the dimensions of the tubes, the pressure, and the concentrations of the two species affected the equations and gave the observed flame profiles. Later, their results were shown to be the asymptotic solution in the limit of large Damköhler number. They do not consider the effects of flow, but many of their assumptions can be validated in the proper asymptotic limits [26].

Zeldovich [27] did preliminary asymptotic work on determining the solution for the species and temperature equations for diffusion flames, examining the reaction zone of the flame, and investigating the kinetics of the chemical reaction. He developed a theory for the temperature in the flame predicting that it should be equal to the stoichiometric flame temperature in the absence of heat losses by radiation and cooling. He noted that the extinction of a non-premixed flame is determined by a lowering of the temperature that results from the finite rate of the chemical reaction. He introduced a first order, Arrhenius term for the chemical reaction and constructed his solution based on two different regions in the flow in an asymptotic like solution.

Fendell [28] developed an asymptotic approach to the problem on non-premixed combustion in the case of an axisymmetric flow (see Figure 2.2). He uses a one step chemical model similar to that used by Zeldovich [27] and explores how Arrhenius kinetics can be used to explain ignition and extinction of flames. In addition, he presents an asymptotic solutions for the limit of small chemical activity (nearly chemically frozen flow) and for a nearly thin flame. Fendell examines the dependence of maximum temperature on the Damköhler number, showing the three branched structure (later described as the 'S' curve

(see Figure 2.3), explaining how the Burke-Schumann model is the limit of Arrhenius ki-
netics as $Da \to \infty$. Liñán continues this model in his work [**29**]. He identifies four zones
from the S curve: a nearly frozen ignition regime, a partial burning regime (unstable), a
premixed flame regime, and a near-equilibrium diffusion controlled regime. The S curve
is a result of high energy asymptotics, as for low activation energy the dependence is a
monotonic function.
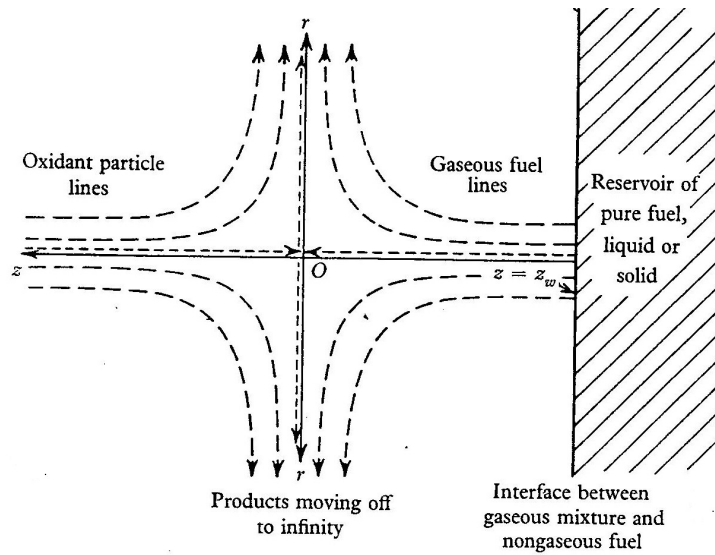
Figure 2.2. Geometry of an axisymmetric flow where oxidizer flows in from
the left, fuel from the right, and there is flame down the centerline where
the reactants join. The products are forced out the side. The dotted lines
refer to particle paths. From Fendell [**28**]

For each identified region in the S curve, Liñán provides approximations to temper-
ature and flame position in his paper, and then he discusses the ignition and extinction
conditions for the flame as related to each region [**29**]. Later work by Liñán and Crespo
[**30**] considers ignition times and shows they depend on the initial thermodynamic state
and chemical kinetic parameters rather than the transport coefficients. Liñán and Crespo
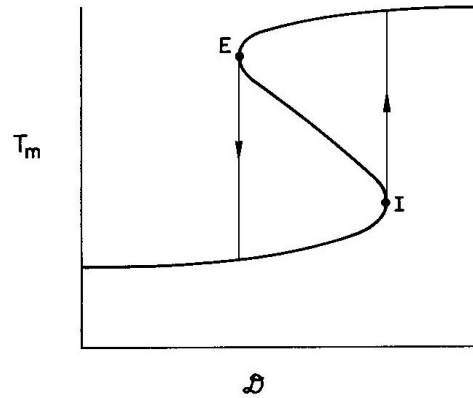
Figure 2.3. A plot of maximum temperature vs Damköhler number with extinction (E) and ignition (I) points marked, typically referred to as the S curve. A similar plot appeared in the work by Fendell [28] and Liñán describes various sections of it in his work [29]. Plot from Buckmaster and Ludford [26]

.

also discuss the asymptotics behind the different regimes in an unsteady premixed flame: ignition regime, deflagration regime, and diffusion regime.

2.2.2. Tribrachial Flames

2.2.2.1. Coflow or traveling flame configuration. A tribrachial flame (or a triple flame as it is more commonly called) usually occurs in weakly stratified or non-premixed conditions. As the flame burns, there is a fuel rich flame that burns on one side, but not all the fuel is consumed. The same happens on the oxidizer side. The unconsumed products diffuse together to form a diffusion flame at the midplane. Buckmaster [31] notes that edge flames also occur in tube-burners, flame spread over fuel bed, and candles burning at low Grashof numbers. Phillips [32] described the characteristic edge flame (he termed it a U shaped front) that he observed propagating along the interface of a methane/air boundary, noting the premixed wings and the diffusion flame along the midplane.

Phillips [32] used a fixed flame, coflow burner and experimentally calculated flame speed discovering it was higher than that predicted by a stoichiometric mixture. He also observed the flow profile noting that the speed of the tracer particles increased as they went through the flame. Kioni, *et al.* [33] also experimented with a coflow burner, showing a stable edge flame where the premixed wings are parallel. They also verify Phillips' observation that flame speeds are higher than the adiabatic laminar burning velocity.

One potential region of interest is that of slowly varying flames (SVF) where one of the Lewis numbers is bounded away from unity. Dold's work models this type of situation [34]. He uses matched asymptotic expansions to find profiles of triple flames with low heat release and in the limit where the propagation speed is near that of the maximum adiabatic laminar flame speed (which he concludes is an upper bound for the flame speed). He concludes that the mixture fraction gradient at the leading edge of the flame controls the shape and propagation speed of a triple flame. Hartley and Dold [22] use numerical simulations to study more rapidly varying triple flames as a result of increased transverse mixture fraction gradient (considering only small heat losses). They develop a theoretical model and use numerical simulation to show profiles of flame shape and speed. Their results show flame curvature is inversely proportional to mixture fraction gradient, and they demonstrate that curvature of the edge flame causes a decrease in speed. While they investigate only regions with positive propagation velocities, they report work where zero or negative propagation speeds were exhibited, and linked flame speed to curvature of the leading edge of the flame. Buckmaster and Matalon [35] study edge flames in the SVF limit, taking the oxidizer Lewis number to be unity and assuming a fuel Lewis number

greater than unity. They also take the upstream concentration gradient to be small and develop asymptotic solutions for both the flame shape and speed. In their work, they seek solutions to a steady propagation into an unbounded regime, but discover instead a situation akin to an anchored flame due to the behavior of the fuel rich branch.

Ruetsch, *et al.* [24] extend the understanding of edge flames by considering the case when there is heat loss. Their numerical work showed how mass fraction, reaction rate, temperature and density profiles for the triple flame (see for example Figure 2.1). They show the importance of heat transfer in edge flames. Behind the wings, the temperature rises, and heat is conducted away from the mid-plane. If too much heat is lost, the edge flame is quenched, but the heat release generates a strain field that resists quenching. They verify the results by Dold under the assumption of zero heat loss; but, they go on to show that the far field flame speed is affected by heat release.

Buckmaster [31] builds on his theory for edge flames propagating through an un-bounded weakly stratified mixture. His theory uses side terms to model heat lost through the boundaries and reaction terms that preserve the fact that equilibrium states are fixed by the Damköhler number and reaction be diffusion limited in the limit of large Damköhler number. He notes that a different asymptotic treatment is needed for different values of the Damköhler number. For large values of the Damköhler number, he develops an as-ymptotic solution to the unbounded edge flame, and compares and contrasts this solution with a classic deflagration wave noting that the deflagration wave will always have a pos-itive propagation speed, while an edge flame can have a negative speed, depending on the Damköhler number. Also, there is no cold boundary difficulty with the edge flame

solution. For order one values of the Damköhler number, he outlines a shooting strategy to find the eigenvalue (related to the speed).

Plessing, *et al.* [36] did numerical and experimental work on triple flames using a complicated (10 step) reaction model. They studied intermediate species and rates of formation and consumption in flames as well as the stability of triple flames and the dependence of the flame on mixture fraction gradient. They present a comparison between experimental and numerical profiles. They determine that at low strain rates, the partially premixed counterflow flame has three reaction zones. As the strain rate increases, these zones merge to be one diffusion flame. Heat exchange and heat losses at the edge determine the structure of a triple flame. Echekki and Chen [37] also did stability studies on triple flames with complex chemistry. They determine that the different chemicals involved in the burning of methanol are responsible for the asymmetric flame shape, partially due to the difference in diffusion rates of the various components.

2.2.2.2. Tribrachial Flames: Counterflow configuration. Triple flames are also observed in counterflow configurations where oxidizer and fuel meet with a flame sheet at the intersection. Figure 2.4 shows a theoretical model of such a situation with the edge flames running perpendicular to the plane of the counterflow from the work by Daou and Liñán [38]. Such configurations depend on strain for the flame sheet to be maintained, and studies of such systems are often analyzed to understand the effects of strain on flames. In turbulent flow, such strains may cause extinction. Buckmaster [31] suggests that there could also be edge flames in premixed flows if there is a counter flow of cold fresh mixture.
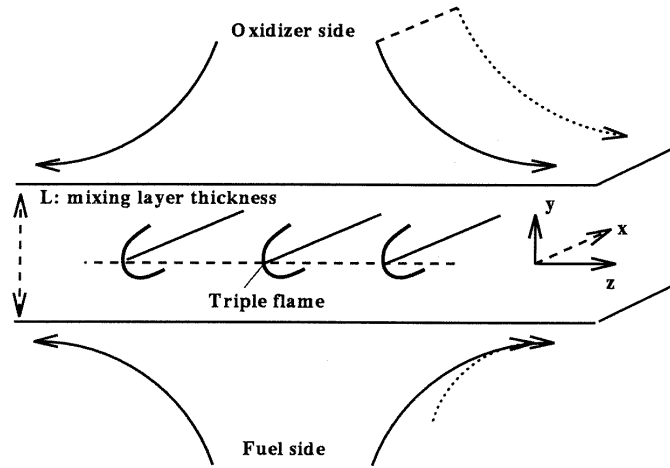
Figure 2.4. Model of edge flames in a counterflow. The edge flames here seem to be coming out of the page. Oxidizer flows from the top, fuel flows from the bottom, and a mixing layer with a flame is formed at the intersection. Figure from Daou and Liñán [38]

Kioni, *et al.* [33] presented theoretical and numerical solutions for an edge flame generated by a strained, steady, counterflow problem. They showed that as the strain rate increases (*i.e.* the Damköhler number decreases), the edge flame transforms into a regular diffusion flame. When the strain rate is very large, the velocity becomes negative, indicating a failure wave rather than a propagation. Buckmaster [31] addresses the model Kioni, *et al.* developed for a counterflow, suggesting improvements. He suggests that the relating the retardation to stretch is a one dimensional phenomena that results from the existence of three equilibrium solutions (the S curve for Damköhler number). Shay and Ronney [39] present experimental work on flows with spatially varying strain to study the effect of strain on quenching. Their work will be further discussed in Section 2.3.2.

Daou and Liñán [**38**] derived expressions for the flame shape and flame speed in the limits of large Damköhler number. They considered the effects of unequal feed temperatures, non-unity Lewis numbers, and different Damköhler number, showing the range of speeds (including negative speeds or failure waves) are possible in certain ranges of Damköhler number and Lewis numbers. They show how decreasing the Lewis numbers causes velocities to increase and present numerical work to supplement their analytical work.

2.2.3. Flame holes and flame disks

Nayagam, *et al.* [**23**] extend Buckmaster's work on one dimensional edge flames to consider flame holes with curved edges. They show that there are no stable free flame holes (*i.e.* one without sinks near the edges). The free flame holes collapse when the Damköhler numberis large. If it is small, there is a critical radius and initial radii larger than these expand while critical radii smaller than the critical radius shrink. Anchored flame holes (those with a heat sink attached) can be stable, depending on the Damköhler number. Under a certain critical Damköhler number, there are no stable flames. They determine that a sufficient gradient in Damköhler number is needed to support a flame hole which, they claim, is why experiments using counterflow jets to produce laminar flow do not exhibit stable flame holes. They also explained how their work can be applied to turbulent diffusion flames, where there is often large gradients in Damköhler number leading to the possibility of flame holes. Also, by examining the Damköhler number in a region, it can be predicted whether a flame hole will grow or shrink.

Potter *et al.* [40], using a tubular burner, were able to observe stable flame holes in a counterflow diffusion flame. They used counterflow jets which have a Hagen-Poiseuille parabolic velocity profile and by increasing the strain rate, they were able to get the holes to extinguish in the center of the sheet and remain stable.

Buckmaster and Jackson [41] continue the work investigating the effects of curvature on flame holes. They examine the dependence of flame quenching on Damköhler number, focusing on the conditions under which they will close. As the radius decreases, the range of Damköhler number for which the hole will not collapse also gets smaller. They also consider what they term a "flame isola" or a island of flame (the opposite of a flame hole– also known as a flame disk). Changes in Lewis number are only pertinent for small holes because they adjust the heat released to keep the Burke-Schumann flame temperature the same. They give a qualitative analysis of edge speeds and argue that the speed is a function of the radius of the hole when the hole/disk is growing. When the radii are large growing disks/holes behave as straight edges.

Pantano and Pullin [42] determine a time dependent, self-similar solution of the one dimensional edge flame model, continuing the work of Buckmaster for large activation energy and unity Lewis number. They note that no self-similar solution is available for non-unity Lewis numbers. They considered holes whose radii were small compared to the thickness of the mixing layer and study the cases where a planar configuration and an axisymmetric configuration are used. They show similar dependence of the solution on Damköhler number as did Buckmaster and Jackson [41]. Also, they show a relationship between the edge flame position and time (which in turn can be used to relate the velocity to the edge flame position or time as will be discussed in a later section). They conclude

that side losses do not affect the leading order solution. Numerical results verifying their analytic conclusions are also presented.

Ghosal and Vervisch [1] present a two dimensional model of a triple flame, following the work of Dold [34] and Hartley and Dold [22]. Where Dold and Hartley considered the flame shape to be unknown, Ghosal and Vervisch assume the profile is parabolic with an unknown curvature (that is determined as part of the solution method). This assumption, while *ad hoc*, allows the development of analytic solutions for the flame's propagation speed, reaction rate, curvature, and temperature in the limits of large activation energy and small heat release. Together with the work of Ghosal and Lu described in the next paragraph, their work will form the basis for part of the work conducted here.

Related to the work with adiabatic walls, Lu and Ghosal [2, 3] found a similarity solution for the problem of two flames colliding in the case of unity Lewis number in the one dimensional case. Lu [3] conducted a numerical exploration of different cases when the Lewis number varied from unity. For unity Lewis numbers, the temperature increases to and then remains at the adiabatic value. When the Lewis number is greater than unity, the flame temperature increases before the flame causing a peak value greater than the adiabatic temperature, while for Lewis numbers less than unity, the temperature decreases from the adiabatic temperature as the flames collide. Figure 2.5 demonstrates these temperature variations. All flames colliding accelerate as they collide; however, for Lewis numbers less than unity the flames show a slight decrease in speed when they first get close to each other before acceleration. An analytic solution for general Lewis numbers in two dimensions will hopefully illuminate some of the interesting behavior discussed by Lu. They also conduct a numerical investigation of flame holes and flame disks in two

dimensions for unity Lewis number [**3, 43**], taking into account the effects of the flow fields and considering temporal evolution of both flame holes and flame disks. When the strain rate is large, the flame collides and forms a diffusion flame since the premixed wings are practically non-existent (as was discussed by Kioni, *et al.* [**33**]). For smaller strain rates, after the collapse the premixed wings become flame isolas and gradually fade away. For flame disks, they discuss the critical radius that divides expanding and contracting regions. The critical radius is dependent on the strain, and increases with increasing strain rate. It can also be related to the energy of the ignition source. We will continue the work done here expanding it to include non-unity Lewis numbers and examine the effects that this has on flame hole collapse.
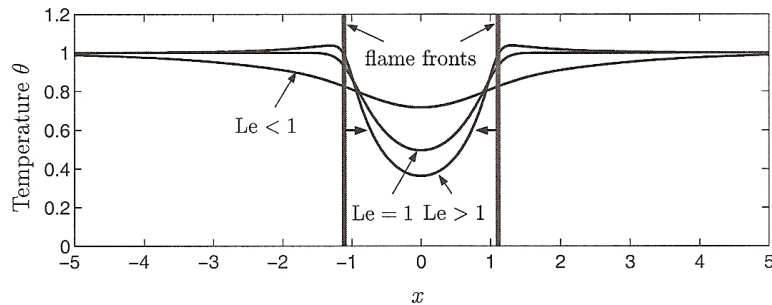
Figure 2.5. Temperature profiles for different Lewis numbers. For unity Lewis number, the flame temperature is the adiabatic flame temperature and remains so behind the flame. For $Le > 1$ the flame temperature is above the adiabatic temperature and for $Le < 1$ it is below the adiabatic temperature. This figure is taken from Lu [**3**]

2.3. Experimental Studies

The main types of burners used in combustion experiments today are the coflow burner, characterized by the combination of fuel and oxidizer in such a way that both

reactants flow in one direction together (for example, see Figure 2.6), and a counterflow burner, where fuel and oxidizer are forced together from opposite directions through jets creating a planar flame (see for example Figure 2.9). A brief description of some of the burners used in various experiments are given in the following sections followed by a brief description of the porous plug counterdiffusion burner that will be the subject of the research that is presented in Chapter 3.

2.3.1. Coflow Burners

Modern diffusion flame experiments can be traced back to the seminal work by Burke and Schumann [25]. Instead of using a Bunsen burner (which is typically a premixed flame), they studied flames from a burner where pure fuel met the air and the flame was created at the interface between the two. This flame, which they referred to as a "diffusion flame" is of interest in diverse circumstances ranging from mining [32] to cooking ranges [44]. Their experimental set up consisted of two concentric tubes, the inner tube carried fuel into a wider chamber formed by the larger tube containing an air flow (see Figure 2.6(a)). This generated a flame that was cylindrical at the base. To get a flat flame, they suggested using parallel plates rather than the tubes. They considered the effects of varying the dimensions of the tubes, changing the coefficient of diffusion, adding an inert gas to the fuel mixture, changing the pressure, preheating the gas, and adding oxygen to the fuel on the flame shape and flame height. Their experiments showed, among other things, that an overventilated flame has a profile that arcs out while an underventilated flame curves in, much like the flame on a candle (see Figure 2.7).
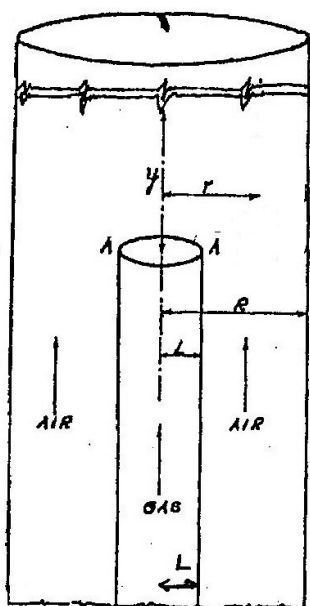
(a) Burke and Schumann [**25**]
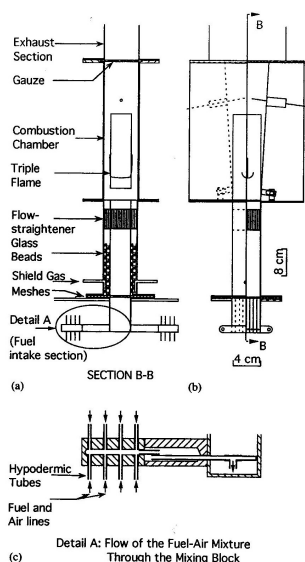
(b) Kioni, *et al.* [**33**]
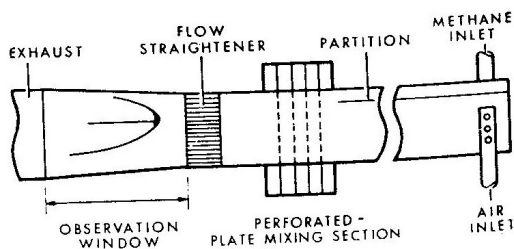
(c) Phillips [**32**]
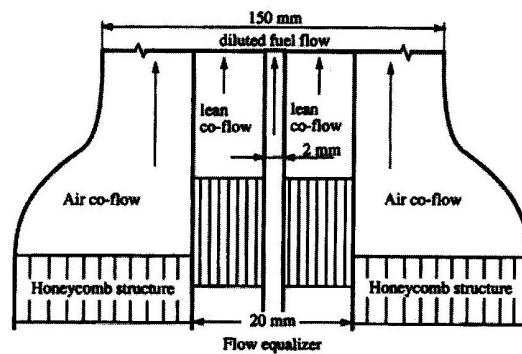
(d) Plessing, *et al.* [**36**]

Figure 2.6.   Coflow burners that introduce fuel and oxidizer by means of channels of initially separate fuel and oxidizer that join. A flame front occurs where the two come in contact in stoichiometric proportions. Some incorporate various methods of mixing (such as glass beads) or flow straightening devices to create uniform conditions.
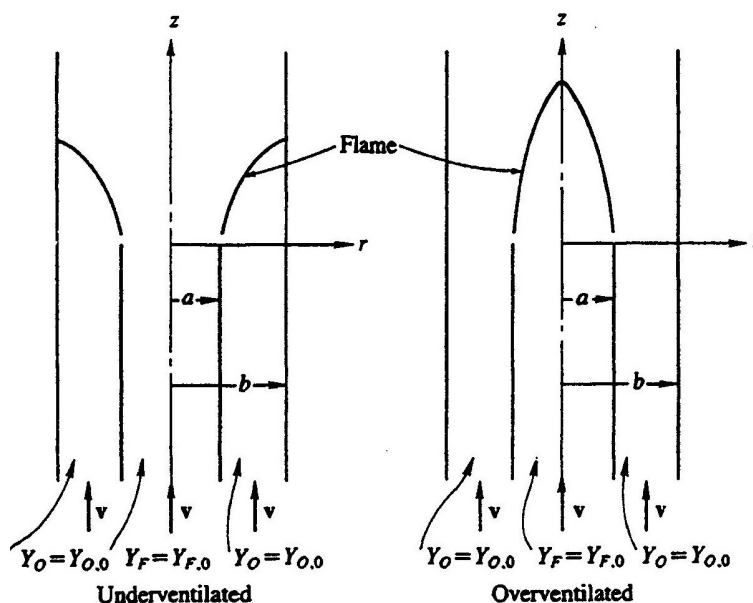
Figure 2.7. The diagram on the right shows an underventilated flame, where there is an excess of fuel and the flame terminates at the wall of the outer cylinder. For the overventilated flame, there is an abundance of oxygen and the flame forms a conical shape, symmetric about the midplane [**25**]. This figure is reproduced from Williams [**9**] based on the work by Burke and Schumann.

Phillips [**32**] analyzed methane flames and was one of the first to publish photographs of edge flames and provide a description of their composition. He used two models for his experiments: one was an open gallery 6 feet long by 4 inches wide and a foot across with glass walls for observation. Methane diffused in through the roof then a spark was ignited at one end causing a combustion wave to travel the length of the chamber. His second experimental apparatus was a static flame rig (see Figure 2.6(c)) where methane and air were introduced into a tube, but separated by a plate. The stream would stabilize before the end of the partition giving a laminar flow before the gases went through a mixing section and a flow straightener. Phillips' experimental work focused on determining flame speed and the quantity of fuel and distribution required to support a flame.

Kioni, *et al.* [**33**] used a variation of the coflow burner used by Burke and Schumann to study strained diffusion flames. The burner uses different compartments to control the mass fraction gradients. Figure 2.6(b) gives details of their burner. Their experimental work focused on the importance of mass fraction gradients and strain in determining velocity and flame structure. They found that velocities produced by their burner were higher than adiabatic laminar burning velocities for a premixed flame.

Plessing, *et al.* [**36**] did work using a coflowing stream with fuel on the inside, then a dilute fuel air mixture, finally a uniform air co-flow (see Figure 2.6(d)). This arrangement provides a three zone structure with an inner, premixed core, an outer fuel lean mixture and a diffusion zone in between to generate a triple flame in a laminar flow. Their work concentrated on measuring velocities, temperatures, and the concentrations of intermediate species and final products.

2.3.2. Counterflow Burners

Counterflow burners can be used to study planar flames under strain for both premixed flames and non-premixed flames. Figure 2.8 from the work of Seshadri [**45**] shows the experimental configuration.

The effect of stretch on flames generated by opposing flows of partially premixed fuel and oxidizer has been studied by Osborne, *et al.* for a better understanding of flame structure and emissions [**44**]. Their apparatus consisted of two jets, one of premixed methane and the other of air, that streamed together and were ignited at the midplane to form dual flames (a premixed flame and a diffusion flame), perpendicular to the plane of the flow (see Figure 2.9(a) for the apparatus and Figure 2.10 for the flame).
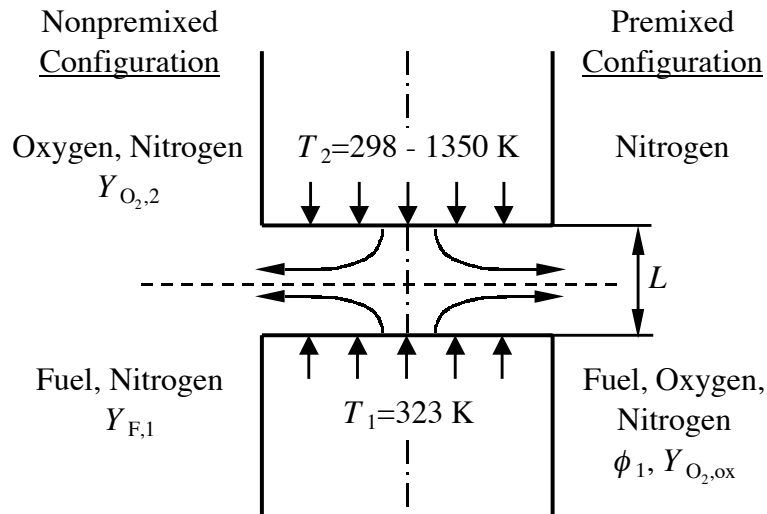
Figure 2.8. Example of a counterdiffusion set up from Seshadri [**45**]. The fuel and oxidizer combine at the midplane to create a flame.
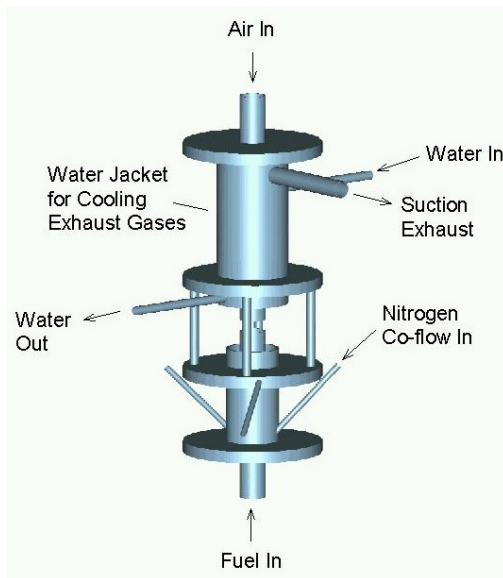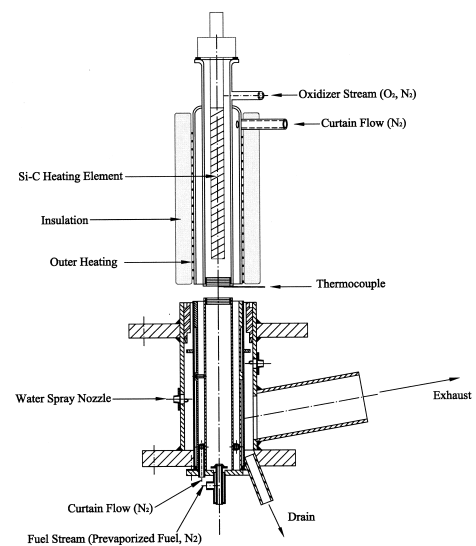
(a) Osborn, *et al.* [**44**]   (b) Seshadri [**45**] and Seiser, *et al.* [**46**]

Figure 2.9. Counterflow burners that introduce fuel and oxidizer as two opposing jets with a flame at the intersection.
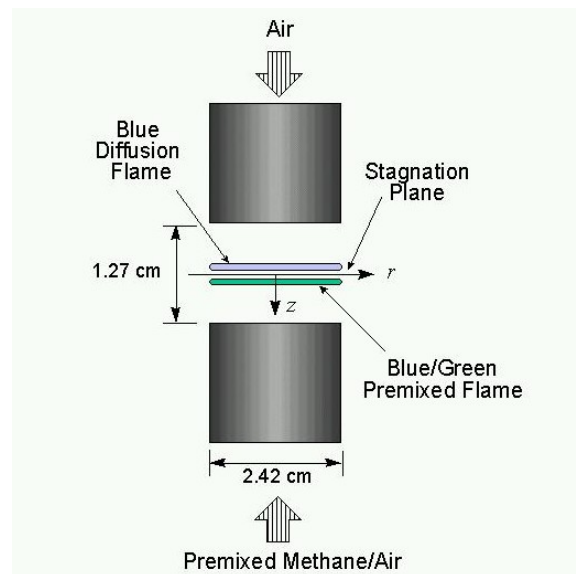
Figure 2.10. Schematic of the dual flames produced by a partially premixed fuel supply and an oxidizer jet. The top flame is a diffusion flame caused by unburned fuel diffusing up to the oxidizer supply and the blue/green lower flame is a premixed flame. Note that both flames are under strain from the burner configuration [44]. Photograph from their website.

Seshadri [45] used a counterflow burner to study the effects of strain and mass fraction on the flame structure and extinction. The experimental set up for both premixed and non-premixed fuels is shown in Figure 2.9(b) where two streams of gases combine at the midplane and then flow out the sides. The fuel is heated on the top by a heating element. For both configurations of flames, he determines experimentally the strain rates and fuel mass fractions for which the flames will extinguish and compares with numerical work [45]. This work uses the same experimental apparatus as the one used by Seiser, *et al.* [46] to study the ignition of hydrocarbons. Shay and Ronney used a counterflow burner to study spatially varying straining flows. By using slightly offset slot jets, they could generate a strain gradient and thus produce a stabilized flame edge. They did not detect oscillations or cellular flame structures near extinction, nor did they find tribrachial flame

structures. They determined from their observations that extinction strain is less for the spatially strained flame than for the uniformly strain flame, and the minimum fuel concentration is larger for spatially varying strained flame [39].

Chen and Sohrab [47] investigated the influence of the Lewis numbers on extinction in a jet counter-flow flame by using methane or butane with nitrogen and burning with an oxygen/nitrogen mix. They found critical minimum values for concentrations at extinction and defined flammability limits for various velocities. As part of their study, they note that the limiting values for these concentrations (*i.e.* in zero strain rate) are finite, but they were unable to reach these values due to the instability in the ultra low strain region.

Han *et al.* [48] have created a low strain rate burner by using a spherically symmetric burner with a large radius of curvature. They consider methane flames and create a flame stability diagram considering the mass flux and concentration of nitrogen. They observe cases of extinction due to heat lost to the burner and radiative heat loss extinction. In addition, they document oscillations observed during the course of their experiments.

2.3.3. Porous Plug Counter Diffusion (PPCD) Burners

Many previous analytic works such as [24, 27, 49, 50] use the assumption of unstrained flames in their examination of diffusion flames. The previous burners discussed all introduce strain by forcing the two components together and that makes it difficult to compare analytical results for unstrained flames to the experiments conducted under the strained conditions. Papas, *et al.* (see [51, 52, 53]) have developed a new burner referred to as a Porous Plug Counterdiffusion (PPCD) burner that allows for nearly unstrained planar diffusion flames that allows for easier comparison with models of unstrained flames. Since

strain rates affect the extinction limits, with the unstrained flame exhibiting the lowest extinction concentrations, the PPCD burner provides an excellent tool for studying the limiting cases of extinction concentrations.

The burner consists of fuel that flows upward through a porous plug and tiny hypodermic needles that bring oxygen in from above and allow it to diffuse down to the flame level. The burner introduces spatial non-uniformities, roughly the size of the diameter of the needles, but after this initial layer, the flow is again uniform. This produces an unstrained flame that allows the product to flow upwards (between the needles) and escape. Figure 2.11 shows a schematic diagram of their burner and Figure 2.12 shows a flat flame in one of the burners. While there is a preferred direction of the flow of gas (similar to coflow burners), the fuel and oxidizer are introduced from different sides of the flame (hence, counter-diffusion).

Theoretical work by Cheatham and Matalon [49] and Kukuck and Matalon [50] predicts cellular structures or oscillating behavior as the flame approaches extinction conditions. Experiments in a strained flame such as those conducted by Shay and Ronney [39] found no such cellular structure, due perhaps to the opposed, angled jets in their configuration. Their counterflow burner was unable to detect these cells, due to both the angle and the strain in their jets. Cheatham, *et al.* studied a flame configuration where the fuel flowed up a channel and oxidizer diffused down, thus providing a configuration with no strain. Products were removed by a stream flowing perpendicular across the top. Figure 2.13 shows their hypothetical burner. The realization of this burner came through a similar design by LoJacono, *et al.* who were able to combine fuel flow, oxidizer diffusion, and product removal in their porous plug counter diffusion burner that produces a flame
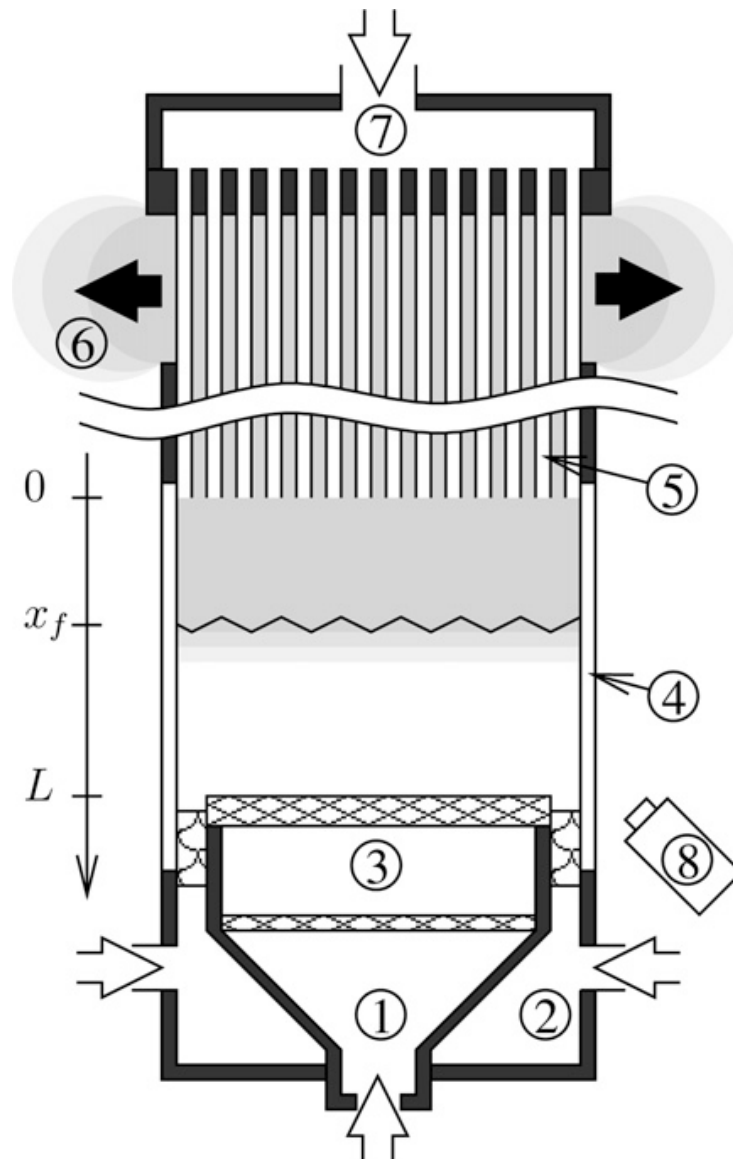
Figure 2.11. Sketch of the porous plug counterdiffusion burner (PPCD) presented in the work of Lo Jacono, *et al.* The fuel comes in the bottom (1), mixes with inert gas (2) then travels through porous plates (3) where the flow is stabilized (uniform profile is assumed). The oxidizer and inert are mixed at the top (7) and the mixture is introduced through a series of needles that come down from the top of the diagram (5), then the oxidizer diffuses down to the flame position (here x_f). The products of combustion are carried up between the needles (6) and the hot exhaust is released at the top of the chamber. The windows of the burner are glass (4). This figure is taken from [**51**]
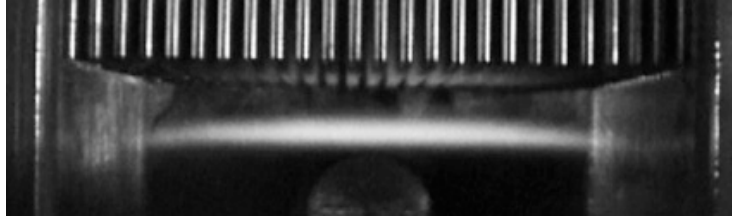
Figure 2.12. An actual porous plug counterdiffusion burner with flame from the work of Lo Jacono, *et al.* Here, they burn "4.348% mass H_2 and 62.92% mass O_2 diluted in CO_2, $Q_O = 3.33 \times 10^{-5} m^3 s^{-1}$" [51]. Each tube is 1 mm.

with small strain. Using this, they were able to experimentally verify the formation of cells near the extinction limit under various conditions and depending on the type of gas used [51].

Another important problem examined using the porous plug counterdiffusion burner is the dependence of extinction on whether the fuel or oxidizer is convected through the flame. In a counterflow burner, the flame location typically lies on the oxidizer side of the stagnation plane for a hydrocarbon-oxygen system; but, the flame cannot be made to lie on the fuel side of the stagnation plane. It is hypothesized that the extinction limits may vary depending on which reactant is diffusing into the flow [49]. Proof that this was indeed the case was supplied through experimental work and corroborated by numerical work. The PPCD burner can be reconfigured such that oxidizer flows up from the bottom and fuel diffuses in from the hypodermic needles or vice versa. Biles, *et al.* [52] have done preliminary work on determining extinction limits in methane flames, showing good qualitative agreement between the asymptotic limit of extinction for both fuel flowing and oxidizer flowing in comparisons between numerical simulations and experiments. They also compared flame position in the burner with the theoretical flame position and showed

Oxidant stream

$x = 0$ — Reaction sheet
$x = x_f$

U
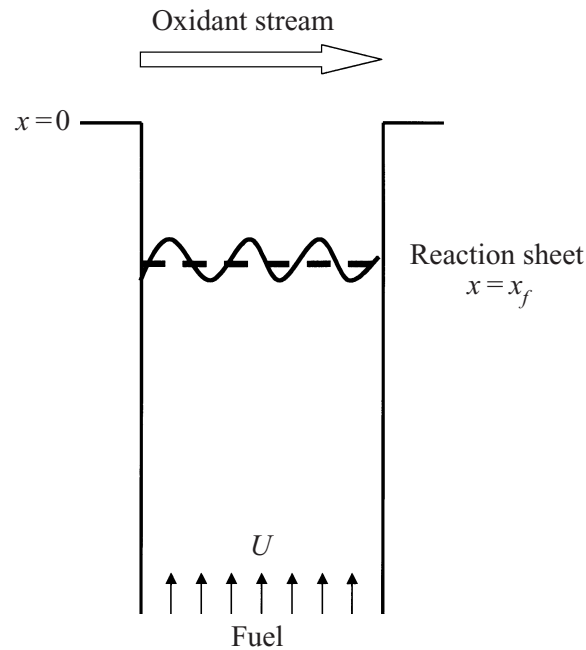
Fuel

Figure 2.13. Hypothetical burner from Cheatham and Matalon [**49**]. Here, fuel comes up the chamber with velocity U, oxidizer diffuses down from the oxidizer stream, and there is a flame at the reaction sheet. Products are removed through the oxidant stream at the top.

that away from the extinction limit, the experiments verify the theoretical work, but as the extinction limit is approached, the experimental curves do not agree with the theory.

In addition to the work mentioned above, having a flame zone that is thick enough to facilitate spatial measurement is an advantage to using the porous plug counterdiffusion burner. Due to the planar nature of the flame, experimental results can be compared to the one dimensional models. Also, this burner gives the ability to control parameters such as bulk flow direction and initial mixture strength independently [**52**], making it very useful for testing theories against experiment.

CHAPTER 3

Extinction of Unstrained, Nitrogen-Diluted Propane-Oxygen and Methane-Oxygen Diffusion Flames

3.1. Introduction

Experiments to study the effects of mass flow on the extinction of unstrained planar flames were conducted using a porous plug, counter-diffusion (PPCD) burner discussed in Chapter 2[1]. Large numbers of studies have been preformed on extinction limits in different configurations of flows; however, only a few provide an unstrained flame to study the limit of extinction. In Section 3.3, my experimental results are presented and the extinction curves for nitrogen diluted methane and propane flames are examined. A more in depth look at the burner configuration, whether fuel or oxidizer convects, is compared with the analytical work previously discussed. Section 3.4 discusses the influence of mass flux on extinction limits. In Section 3.5 a study of the oscillations observed in methane and propane flames is discussed, providing experimental data and quantification of types of oscillations and descriptions of their onset. How the oscillations affect extinction is also discussed.

In addition to the experimental work, Biles, Jakulewicz, Papas and Goodwin have numerically simulated combustion in the PPCD burner using a complex chemical model

---

[1]Experiments were conducted at Colorado School of Mines in the lab of Prof. Paul Papas from January 2006 through August 2006.

[**52**], and now the goal is to bridge the gap between complex chemistry models and analytic models that assume one step chemistry (see for example Matalon, Ludford, and Buckmaster [**54**]) by conducting simulations using one step chemistry models and detailed transport descriptions. In Section 3.3 extinction simulation results are presented with comparisons between experiments and numerics, and a comparison between simple chemistry and complex chemistry is shown. Through comparison, it is possible to extract important experimental parameters such as reaction order and activation energy. The ultra low strain rate on the flame sheet is of key importance to this work. Most complex chemistry simulations of practical configurations require immense calculation, and involve multidimensional flow fields (*i.e.* hydrodynamic strain). Removing strain reduces the number of uncertainties to focus the attention on the effect of chemistry and transport in combustion.

3.2. Methods

3.2.1. Experimental Methods

Extinction experiments were conducted on the porous plug, counterdiffusion (PPCD) burner, designed to experimentally realize a counterdiffusion flow as described by Matalon *et al.* (see for example [**54, 49, 50**]). The burner consists of a walled chamber, $0.077 \ m \ \times 0.021 \ m \times 0.087 \ m$, with glass on three sides and a brass backing (see Figure 3.1 for photograph and Figure 2.11 for a detailed schematic)). The brass backing has a removable plug that is used to light the burner and can be used to hold a thermocouple for temperature measurements. When running, this plug is inserted, completing a solid wall

on the back side of the burner. A porous plate is on the bottom and an array of hypodermic tubes (diameter $= 1\ mm$) on the top. One reactant convects from the bottom, where it passes through a porous plate, to the top where it escapes out into a vent in the lab and this forms the primary flow. At the top, an array of hypodermic tubes supplies the other reactant which must diffuse against the bulk flow of gas to reach the flame. There is a small entrance region on the order of a millimeter where the flow from the tubes into the flowing product gases is non-uniform, but below that the reactant coming from the tubes diffuses uniformly. The products, unburned reactants, and inert gases escape up the top of the apparatus through gaps in the tube array. Since the burner is not pressurized, the interior of the burner is near atmospheric pressure. Either fuel or oxidizer can be fed from the top or the bottom of the apparatus. Both fuel and oxygen can be mixed with an inert gas (usually nitrogen), and this mixture is what is referred to here as "fuel" or "oxidizer". The relative percentages of fuel (oxidizer) in the inert determines the concentration of fuel (oxidizer). Using a Labview flow control algorithm, flow meters control the relative percentages of oxygen, fuel, and inert introduced into the system as well as the flow rates passing through the burner and the tube array. The volumetric flow rate is the amount of gas flowing through a particular end of the combustion chamber (either the tube arrays or the porous plate). There are two main configurations used in these experiments. Fuel convecting indicates that fuel was introduced to the chamber through the porous plate and was introduced as the primary convection. In this case, oxidizer was introduced through the tubes at the top of the burner and, after a small distance downstream of the tube array exits, diffused against the bulk flow. The case of oxidizer convecting is the opposite: the oxidizer was introduced through the porous plate, convected upward, and

fuel diffused against the bulk flow from the tubes. Flow rates are given in standard liters per minute ($slpm$). In this work, m_f will be used for the volumetric flow rate of fuel mixture and m_o for the oxidizer mixture.
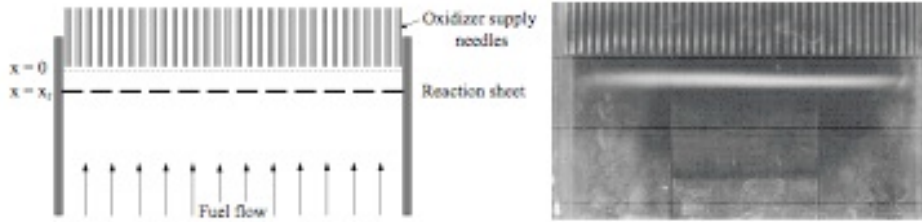
Figure 3.1. Schematic of PPCD burner (left) and photograph of PPCD burner (right) with methane flame (front view). Here 18% CH_4 is diluted with N_2 and burns with 100% O_2. One hypodermic tube has a diameter of 1 mm. The oxidizer is supplied through the needles, the reaction sheet (flame) is visible a few millimeters off the tubes and the direction of convection comes from the bottom. Figure taken from Biles *et al.* [52].

For the experiments all flows are relatively slow flows with flow rates under 2 $slpm$. Unless otherwise noted, the volumetric flow rate from the tubes was kept constant at 1.9 $slpm$ to keep the flame sufficiently far away from the tubes. Nitrogen was used as an inert, pure oxygen as the oxidizer, and either propane or methane for the fuel. Often, obtaining a consistent extinction curve for a stable laminar planar flame required altering the convecting flow rate as the concentrations were varied to maintain the flame position at a reasonable ($\sim 2 - 3mm$) distance from the tube array exit. This will be explored in later sections and appropriate notation will be presented to let the reader know if the volumetric flow rate were kept fixed or varied. The terms "convecting" and "flowing" are used interchangeably through this dissertation.

Concentrations refers to the mole fraction of the gas and are expressed as percentages by volume. The term "extinction concentration" will be used to describe the critical reactant concentration at extinction, *i.e.* the minimum concentration necessary for burning. Exceptions to this standard will be noted. Through this work, the terms "rich" and "lean" will be used to describe the overall mixture strength of the system. Fuel rich refers to cases where the initial concentration of fuel greater than stoichiometric. Fuel lean refers to cases when concentration of oxidizer greater than stoichiometric.

An extinction experiment is conducted as follows. Initially, a flame is lit with fuel and oxidizer conditions set well away from the extinction values. The system then is allowed to equilibrate. To run a case to extinction, the concentration of the reactant under investigation is lowered using small step sizes. After each step, the system must be allowed to return to equilibrium before being lowered again. A run is conducted where the concentration is decreased by 0.01% every 30-60 seconds. During this process, the flow rate is kept constant by increasing the percentage of nitrogen so that the same flow rate is maintained during the entire experiment. Since both methane flames and propane flames are visible when burning, extinction is recorded when the flame is no longer seen. For fuel rich cases, oxidizer is lowered until extinction is reached, and for fuel lean cases fuel is decreased until extinction is reached.

3.2.2. Numerical Model

3.2.2.1. Flame Code. Numerical simulations were conducted using the software package Cantera, written by Dave Goodwin [55]. This software can be executed using Matlab, Python, or C (here, Matlab was used) and is designed to study chemically reacting flows.

It is able to incorporate multiphase chemical reactions, one dimensional flames, reaction path diagrams, and other features essential to modeling combustion [55]. The Cantera model was designed to mimic the experimental apparatus (see Figure 3.2).
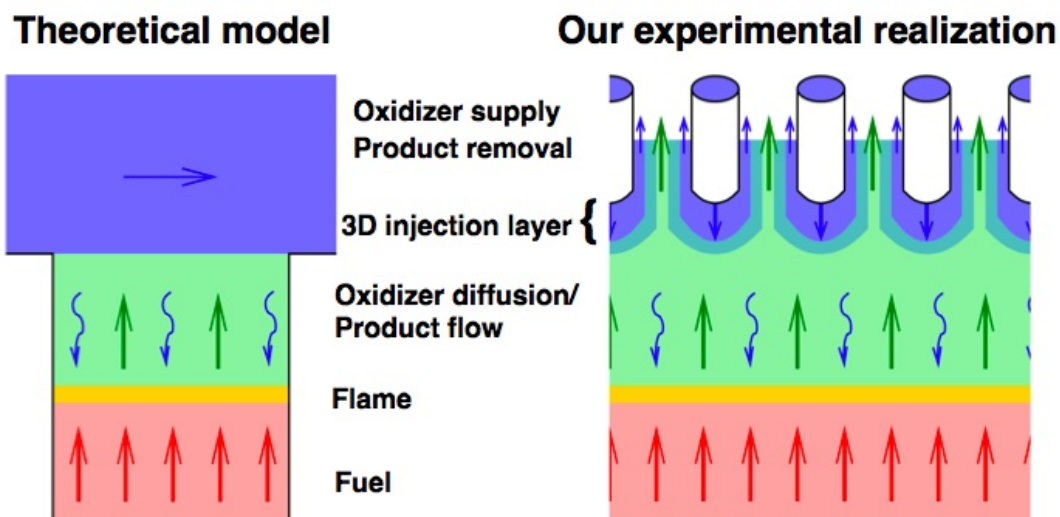
Figure 3.2. Schematic of theoretical model simulated by Cantera (on the left) vs the experimental apparatus (on the right). In the theoretical model, the oxidizer supply reservoir is able to supply the entire amount of pure oxidizer without the constraint of removing the products of combustion. Illustration modified from the thesis of LoJacono [56].

The flame model is controlled by a master code[2] that takes information from different files, including a chemical reaction mechanism, a thermodynamic data base, and a transport data base. Initial conditions for temperature and concentration, and boundary conditions are imported and then executed by Cantera (documentation of this code is available on the web from Dave Goodwin [55]). In Cantera, the one-dimensional energy equation with the species equations is solved assuming low Mach number and nearly constant pressure. Fick's and Fourier's Law are assumed. Cantera uses a variant of Newton's

[2]Originally drafted by Steve Biles and Dave Goodwin [52] and modified by Jocelyn Renner.

method with a time-stepping algorithm to solve the equations. A solution (temperature and concentration profiles) is generated and saved. The boundary conditions that it accesses are designed to model that of a uniform convection on the bottom and a reservoir at the top that emulates a cross flow carrying products away so rapidly that the conditions at the top are considered to be those of the reservoir. (For a better understanding of the theoretical model see [49]). The user can specify the fuel, oxidizer, and inert. As in the experimental case, the pressure is taken to be atmospheric. An ideal gas mix is assumed and effects of gravity are ignored.

The reaction mechanism file has the reactions with the corresponding rates, and exponential factors and follows the Chemkin format with a reaction k defined by the activation energy E, pre-exponential factor A and power n:

$$(3.1) \qquad k = AT^n \exp\left(-\frac{E}{RT}\right).$$

Here, E has units of $\frac{cal}{mol}$ and A has appropriate units found from the balanced reaction. For the complex chemistry runs, GRIMech 3.0 was used [57]. This mechanism has 53 species and 325 different reactions with corresponding rates, activation energies, and pre-exponential factors. The simple runs (primarily used here) have one reaction. For methane this is:

$$CH_4 + 2O_2 \Rightarrow 2H_2O + CO_2$$
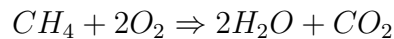
with an activation energy of $E = 4.5 \times 10^4 \frac{cal}{mol}$ (from Puri and Seshadri [58]) and a pre-exponential factor of $A = 3.0 \times 10^{22} \frac{cm}{mole\ s}$ (compare with Puri and Seshadri, $A = 8.9 \times 10^{18} \frac{cm}{mole\ s}$ [58]). The numerical curve was calibrated to match the curve in one place

(oxidizer mole fraction of $X_{O_2} = 0.8$ when fuel is convecting) with the curve generated by GRIMech 3.0. For propane this reaction is:

$$C_3H_8 + 5O_2 \Rightarrow 4H_2O + 3CO_2$$
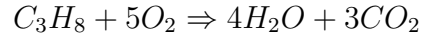
with an activation energy of $3.5 \times 10^4 \ \frac{cal}{mol}$ and a pre-exponential factor of 7.0×10^{35} (compare with Puri and Seshadri $A = 2.9 \times 10^{19} \ \frac{cm}{mole \ s}$ [58]) which was calibrated off of the experimental results at 100% oxygen when fuel is convecting.

3.2.2.2. Boundary and Initial Conditions. Due to simplification including axisymmetric flow, the code is essentially one-dimensional with the length of the domain studied corresponding to the length of the burner ($5 \ cm$).

For the flow, the default is an axisymmetric convection with specified mass flux at the inlet and outlet. The code allows the user to specify whether fuel or oxidizer is convecting. Cantera simulations only have one flow rate, considered to be that of the bottom (*i.e.* in the direction of flow). In the program, mass flux m is given in $\frac{kg}{m^2sec}$. Exceptions to this are noted appropriately. In general, a mass flux of $m = 0.01 \frac{kg}{m^2sec}$ was used for numerical simulations and exceptions to this will be noted.

The concentrations at the boundaries are set to be that of a gas with constant temperatures and constant concentrations. The inlet is taken to be an "AxisymmetricFlow" object from Cantera's database. In addition to being axisymmetric, it is assumed to be one-dimensional with no radial velocity. The number of grid points is typically around 300 points. The grid is adaptive so it adjusts to meet specified mathematical requirements (grad, curl).

In the code, it is possible to model the exit concentration as a reservoir of constant gas properties (oxidizer if fuel is flowing and fuel if oxidizer is flowing), with the product concentration specified to be zero at the exit reservoir. Note that for experiments, when the concentration of the diffusing reactant is 100%, that is indicative of only that reactant (no nitrogen) being supplied through the needles and this is modeled by using a boundary condition of 100% of that reactant at that boundary in a simulation. Realistically the boundary in the experiment will never be at 100% since the products must be handled through the tube array. In the reservoir, axial symmetry is again imposed with zero radial velocity; but no mass flux is imposed (instead it matches the inlet).

Temperatures at the boundaries were specified as

$$T_{\text{inlet}} = 300 \ K \qquad \text{and} \qquad T_{\text{outlet}} = 700 \ K$$

which were chosen to match approximate experimental inlet and outlet temperatures as recorded for an average run. Initially, a flame sheet with a maximum temperature T_{max} corresponding to equilibrium temperature of the mixture was established, then the code was run until a steady state was reached. This flame sheet was used as the initial condition for the simulations. It is important to note that the boundary conditions for the experiment are different than those numerically imposed. In the experiment, there is heat lost from radiation and more importantly to the upper tubes, manifold, and side walls. In the numerics, these heat losses are not accounted for and thus, calculated flame temperatures can be higher than observed temperatures. Also, the product concentration in the experiment at the upper tube array is not zero.

3.2.2.3. Extinction Simulation. Using the inputs described above, the program then first attempts to solve the flow with fixed temperatures, then the energy equation with adaptable grids, and finally it outputs the requested converged solution information *i.e.* plots of temperature and species profiles.

Using a controlling code, numerical simulations were executed in which fuel and oxidizer concentrations were specified at the reservoir and in flow boundaries and sent to the previous described program. A flame solution is generated and the temperature returned. The concentration is gradually decreased and the process is repeated until extinction is reached (modeling a similar procedure used in experiments). The code is adaptive so that initially the step size decreases the reactant mole fraction by 0.04, then at certain specified temperatures (which can be set near the extinction temperature) it decreases to 0.002, and at a lower temperature decreased again to 0.0004. Extinction corresponds to a rapid drop of the maximum temperature from burning (usually around $1200\ K$) to the cold, unreacted solution ($\sim 700\ K$).

3.3. Extinction Curves for Propane and Methane

Extinction curves are the boundaries between region where burning can occur and the region where conditions cannot support a flame. Typically, these curves are plotted as functions of the concentration[3] of the fuel versus concentrations of the oxygen, and the fuel and oxygen concentrations asymptote to constant values. Extinction is influenced by many factors, such as strain rate, concentration, and even the type of fuel being combusted, many of which can be studied through Damköhler number effects. Figure 3.3 shows the results of Cantera experiments on counter-flows run by Biles and Papas

---

[3]Which can be expressed as mole fraction X, mass fraction Y, or percent composition.

[personal correspondence] as well as the results of the experimental results of Yahagi *et al.* [**59**]. The numerical results show three different jet exit velocities $v_{F,O} = 0.25$, $v_{F,O} = 1.00$ and $v_{F,O} = 4.00$ m/s[4] and agree reasonably well with experimental results. In the PPCD burner and related numerical extinction simulations, the influence of strain on these extinction values is practically zero. Since strain rate acts to increase the necessary concentrations to support burning, the limiting extinction values occur at the asymptotic limit of the counter-flow curves when the velocity at the exit is zero and thus the strain rate is zero. This case represents the largest burning region available.
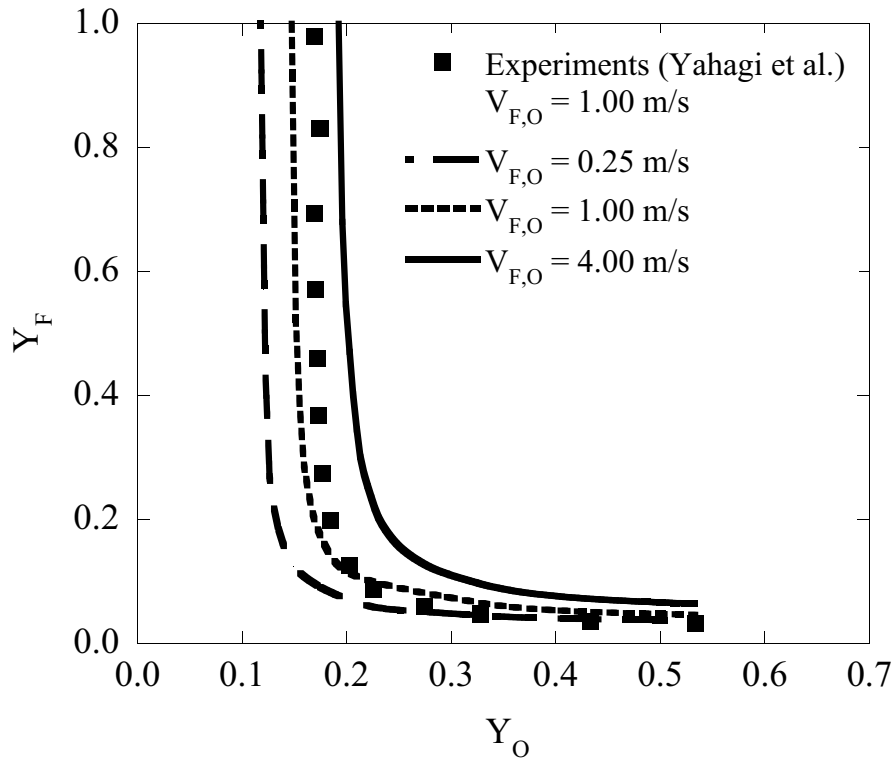
Figure 3.3. Numerically simulated extinction curves for methane burning with oxygen in a counter-flow diffusion configuration with nitrogen as an inert. Experiments from Yahagi *et al.* [**59**]

[4]Here the subscripts F and O refer to fuel and oxygen, respectively.

3.3.1. Experimentally Determined Extinction Curves

The experimentally determined extinction curves found during the course of these experiments (Figure 3.4) are the limiting cases for extinction over a range of flow rates[5]. Since the flames are unstrained, they extinguish at the lowest possible concentration, providing a lower bound to other experiments that have looked at strained extinction of flames (for example Chen and Sohrab [47]). Figures 3.4(a) and 3.4(b) show experimentally determined extinction curves for methane and propane, respectively, that are obtained from the optimal flow rates.

The fuel rich regime is difficult to investigate as the flame approaches the tube arrays as the convecting gas (either fuel or oxidizer) concentration is diminished, assuming the diffusing reactant concentration at the tubes is kept the same, and flame oscillations occur (see Section 3.5). Eventually the flame enters the tube array or extinguishes. Thus, the fuel rich curve (especially with fuel convecting) is incompletely rendered.

3.3.2. Numerically Simulated Extinction Curves

As discussed in the Section 3.2.1, the extinction curves generated numerically are simulations of the experiments conducted in the lab. Numerical simulations were calibrated by changing the pre-exponential factor of the reaction rate such that one point of the extinction curve matched a value obtained from another source. For methane, the numerical curves were calibrated off the complex chemistry model using GRImech 3.0 so that, when fuel is convecting, the fuel concentrations at $X_{O_2} = 0.8$ were identical. For propane the numerical curves were calibrated off the experiments at 100% O_2. Once

---

[5]The importance of flow rate in extinction curve calculations will be discussed later
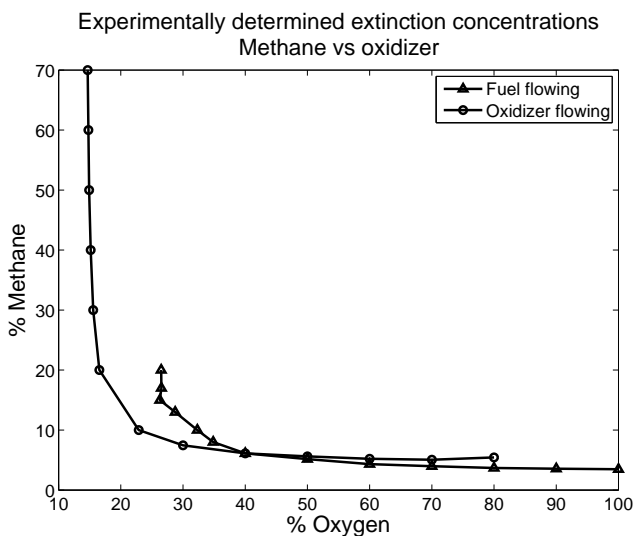
(a) Methane with oxygen, extinction curves
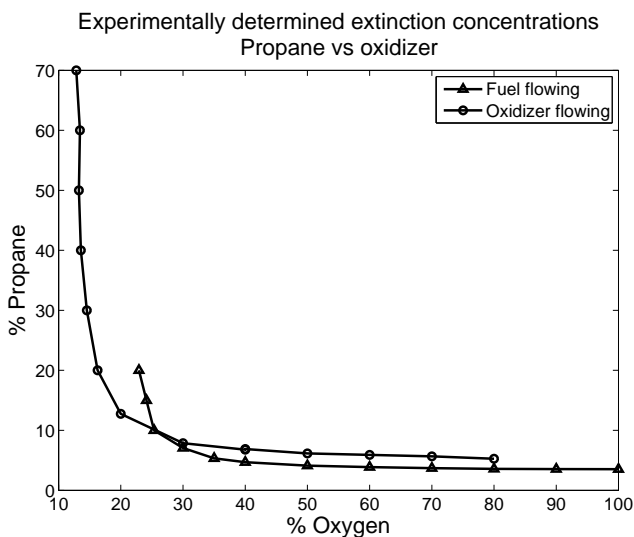
(b) Propane with oxygen, extinction curves

Figure 3.4. Experimental extinction curve for (a) methane and (b) propane showing the concentration of fuel versus the concentration of oxidizer at extinction. Burning occurs above and to the right of the curves. Below and to the left there is no burning. Shown are the lowest concentration values at extinction (regardless of flow rate) for oxidizer convecting and fuel convecting. In all cases, the diffusing reactant had a flow rate of 1.9 *slpm*. The lack of data on the fuel rich side of the curve for fuel convecting is due to the flame's proximity to the tube array.

a pre-exponential factor was obtained, the full curve could be explored without further changes in pre-exponential factor.

Comparisons with the Cantera generated curves for methane using full chemistry and those generated using a one-step reaction show the general trends are independent of chemical models (see Figure 3.5), justifying the use of simple chemistry models in theoretical work. Using a one-step model is computationally faster than the complex chemistry, and the one step model uses the same chemical approximations (one step, fuel + oxidizer reacts to form product, and global Arrhenius rate) as the theoretical models. The slight bend of the curve away from the asymptotic limit on the fuel rich branch (where the mass fraction of fuel approaches unity: $Y_F \rightarrow 1$; see Figure 3.5) is most likely due to interactions with the boundaries in the numerical simulations. The physical experiments could not be conducted in this region due to the interaction of the flames with the tubes. Note, that the bend is greater for the fuel convecting case than for the oxidizer convecting case, as is expected from analysis of the experimental results, most likely because the numerical flame is too close to the reservoir boundary, where conditions at which are kept constant, and boundary effects are influencing the extinction.

The numerically simulated extinction curves for methane and propane, shown in Figure 3.6 show the same basic trends as the experimental curves. As previously mentioned, the fuel rich regime is difficult to investigate both numerically and experimentally. The close proximity of the flame to the tubes is a primary reason that the curves tend to curve away from the expected asymptotic values on the fuel rich side of the concentrations at extinction plot (see for example of the curving away from the asymptotic value, Figure 3.6(a)). In this case, it is observed that on the fuel rich side of the flame when fuel is
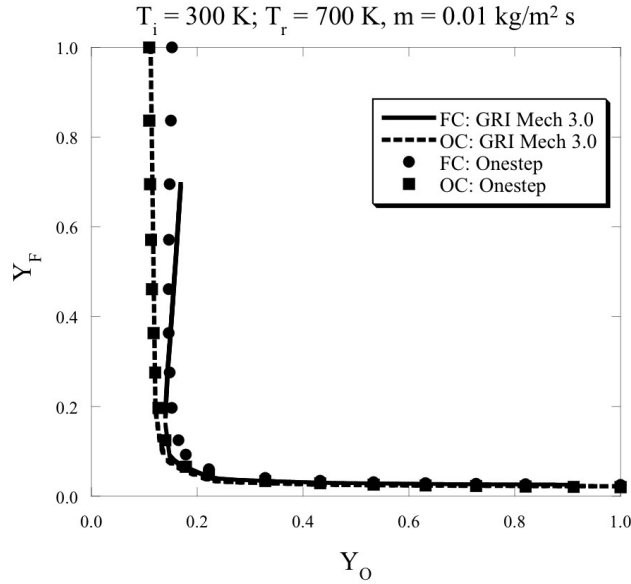
Figure 3.5. Extinction curve for methane and oxygen showing the mass fraction of methane and the mass fraction of oxidizer, generated using Cantera. Lines indicate full chemistry model (GRI Mech 3.0) and the dots/squares indicate points generated using the single step chemistry model. Here, the inlet temperature is 300 K, the outlet temperature is 700 K, the mass flux is 0.01kg/m^2 sec and the dilutant is nitrogen. Note that the single step model has the same trends and the complex chemistry model for both cases of fuel convecting (FC) and oxidizer convecting (OC).

convecting, the flame is very close to the tube array (when the mass flux is $0.01\frac{kg}{ms^2}$ the flame is less than 0.01 mm away from the tubes, see Figure 3.7 for a plot of extinction concentration vs. convecting species). This proximity to the boundary with its imposed temperature could be a reason that there are higher oxidizer extinction concentrations than those observed experimentally and thus why a slight bend is observed in the numerical data. When the flow rate is decreased, the flame moves away from the tubes (see Figure 3.7, and the oxidizer concentration at extinction drops to a minimum, then it increases (see later discussion of this in section on flow rate effects). If heat is lost to the

boundary, then the flame extinguishes faster. In comparison, when oxidizer is convecting, the fuel lean side of the curve is close to the tubes (around 0.02 mm away from the tubes). It is both experimentally and numerically observed that the flame is further away when oxidizer is convecting through than when fuel is convecting through at similar conditions, and this could explain why, numerically, the oxidizer curve exhibits less of a bend than the fuel convecting curve (notice the differences between fuel and oxidizer curves in Figure 3.6). Note that the oxidizer curve[6] with the oxidizer convecting must be compared with the fuel curve for the fuel convecting and visa versa. Numerically, it is observed that as the flow rate is varied, the flame position drops nonlinearly away from the tubes. For a while, it remains near the tubes, then it falls off suddenly.

3.3.3. Effect of Burner Configuration on Extinction Concentration

Cheatham and Matalon predicted differences in extinction concentrations depending on whether fuel or oxidizer was flowing [**49**], and experimentally it is observed for both methane and propane fuel rich cases that the flame extinguishes at a lower concentration of oxygen when oxidizer is convecting than when fuel is convecting (see Figure 3.4). On the fuel lean side of the curve, the flame extinguishes at a lower concentration of fuel when fuel was convecting than when oxidizer was convecting. There is a cross over point at which the system extinguishes at the same concentration for both fuel and oxidizer convecting. This trend is observed for the propane system with the Cantera plots (see Figure 3.6(b)), but not for the methane system (see Figure 3.6(a)).

---

[6]The oxidizer curve simply refers to the concentration of oxidizer at extinction vs flame position
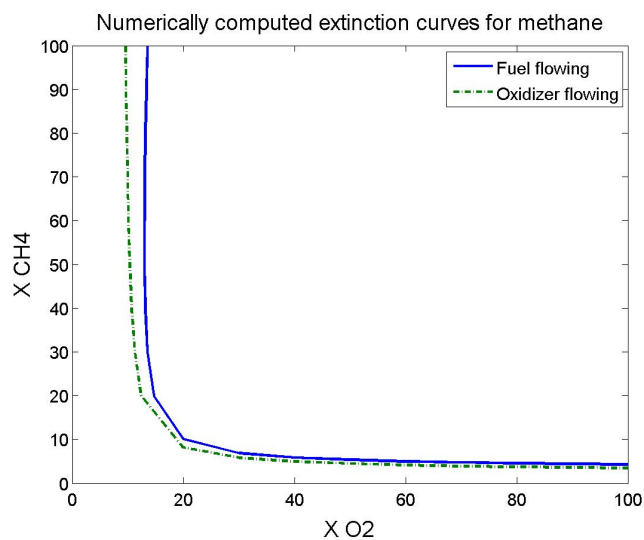
(a) Methane extinction curves
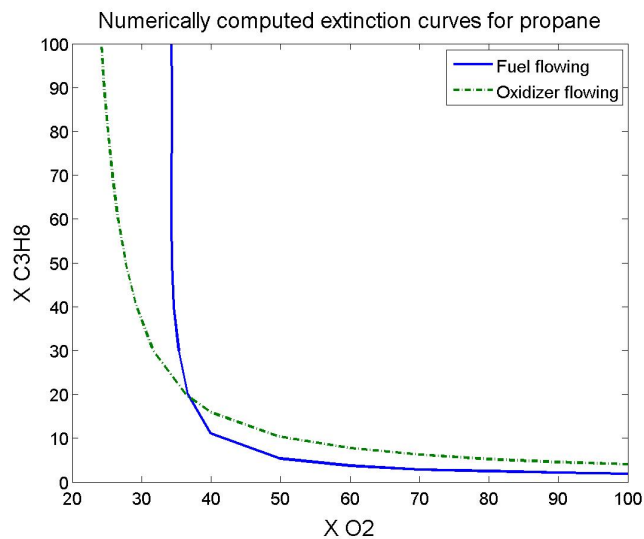
(b) Propane extinction curves

Figure 3.6. Numerically generated extinction curves for (a) methane and (b) propane showing the minimum extinction concentrations. Curves were generated using one step chemistry models.
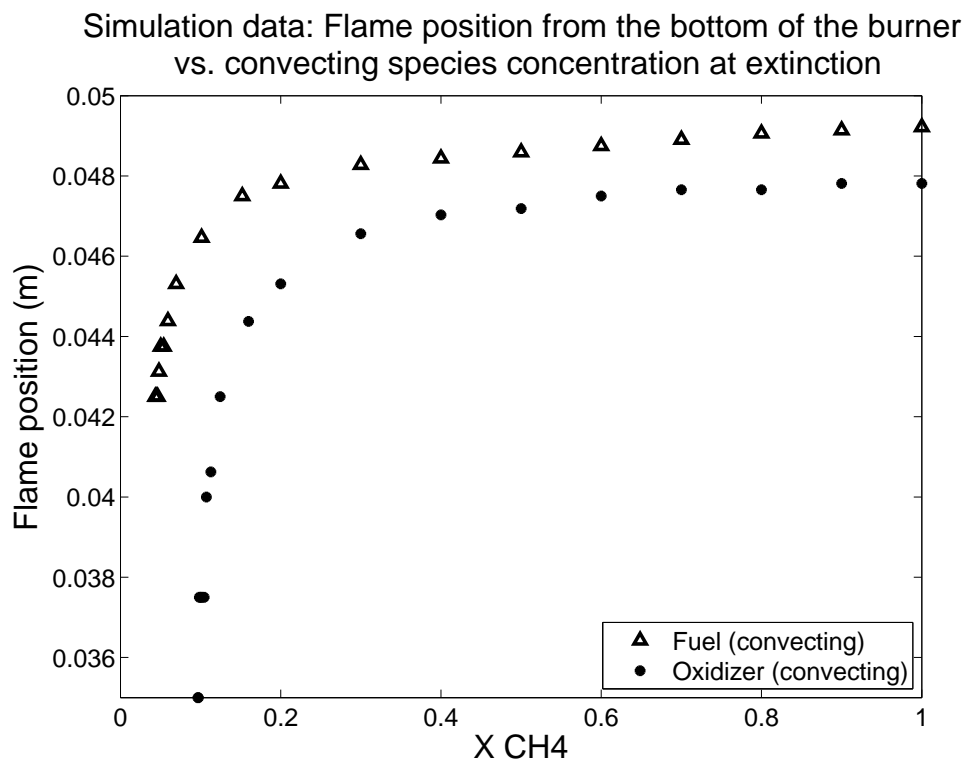
Figure 3.7. Simulation data of flame position from the bottom of the burner vs. extinction concentration of the convecting species (fuel when fuel is convecting and oxidizer when oxidizer is convecting) in the Methane-Oxidizer system. Here, the flow rate is $m = 0.01 \; \frac{kg}{m^2 sec}$, the inlet temperature was 300 K, the outlet temperature was 700 K. The tube array is located at 0.05 m.

3.3.4. Comparison Between Propane and Methane

It is useful to examine the importance of the Lewis number[7] on the extinction concentration using the relationship between propane and methane since methane has a lower Lewis number than propane. Experimentally, it is determined that when fuel is convecting through the system, propane extinguishes at a lower concentration than methane (compare Figures 3.4(a) and 3.4(b)), but this effect is nearly negligible in extremely fuel

[7]The Lewis number is a ratio of the thermal diffusivity to the mass diffusivity, and it arises out of the non-dimensionalization of the species equations.

lean cases. Conversely, when oxidizer is convecting, the differences between the two fuels is much less pronounced, but still propane extinguishes at a lower concentration (on the fuel rich side) than methane. On the fuel lean side, methane extinguishes at a lower concentration. Most likely the differences between extinction limits between the two fuels is due to thermochemical properties of the different fuels.

3.4. Dependence of Extinction Concentration on Mass Flux

It is essential to understand how mass flux affects extinction to determine the validity of comparison between different extinction regimes since the burning regime varies for different ranges of fuel and oxidizer concentrations at different flow rates. If the flow rate is too high, the flames burn in the tubes or near the boundary. Flow rates also affect extinction through the onset of instabilities since many instabilities are related to either low or high mass fluxes. The flow rate is proportional to the mass of fuel or oxidizer reaching the flame plane, which in turn affects the temperature at the flame zone and the reaction rates. Therefore, being able to quantify the differing effects of changing the concentration and changing the mass flux is key to describing flame extinction. Corresponding with expectations, all the experiments and numerical simulations conducted during the course of this study indicate that extinction concentration is highly dependent on flow rate and on burner configuration.

3.4.1. Experimental Results

During the course of the experiments, the flow rate at the tubes was kept constant, usually at 1.9 slpm, to insure the flame stood as far off the tubes as possible. Varying the top

flow rate would allow for stable burning when the bottom flow rate is also decreased. For the purposes of this discussion, assume the top flow rate is constant, and the discussion that follows relates to varying the flow rate at the porous plate.

With fuel convecting and high oxygen content, both methane and propane are stable for high flow rates through the porous plate (flow rates close to that of the oxidizer coming through the tube array). Figure 3.8 shows the dependence of extinction concentration of fuel vs volumetric flow rate of fuel. As the flow rate is decreased, the flames become increasingly unstable, and hence, extinguish sooner. Note that the curve asymptotes (at higher flow rates) to a constant value that is the lowest extinction concentration that can be achieved for this configuration. Ideally, curves like this should be developed for each region and the asymptotic value (*i.e.* the one without oscillations) used for gathering the data on extinction. Practically, there are regions where there may not be combinations where oscillations are not observed, so the best possible approximation must be made. This trend is observed for both methane (see Figure 3.8(a)) and propane (see Table 3.1 or Figure 3.8(b)).

Propane Extinction Conc. (%)	Vol. Flow Rate (slpm)	Oscillations
3.29	1.4	no
3.42	1.2	no
3.53	1	no
4.84	0.8	yes
8.04	0.6	yes
13.91	0.4	yes

Table 3.1. Extinction concentrations for given volumetric flow rates of propane when fuel is convecting. Here, the volumetric flow rate of oxidizer at the tubes was 1.9 *slpm* with X $O_2 = 80\%$. The rise in extinction concentration is closely tied to the onset of instabilities.
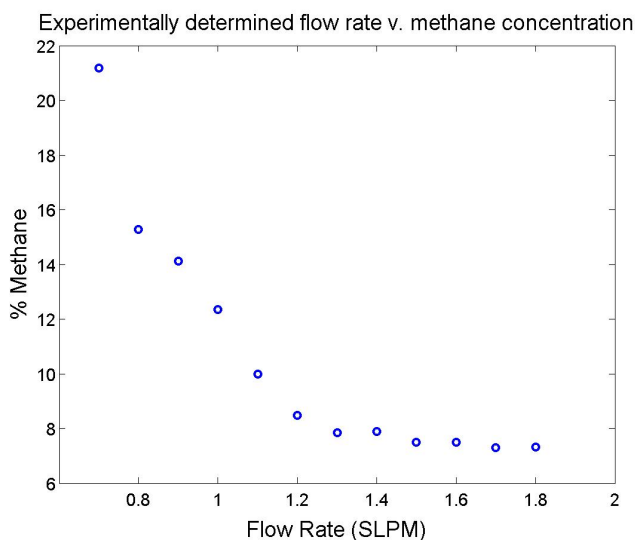
(a) Volumetric flow rate vs. extinction concentration: methane
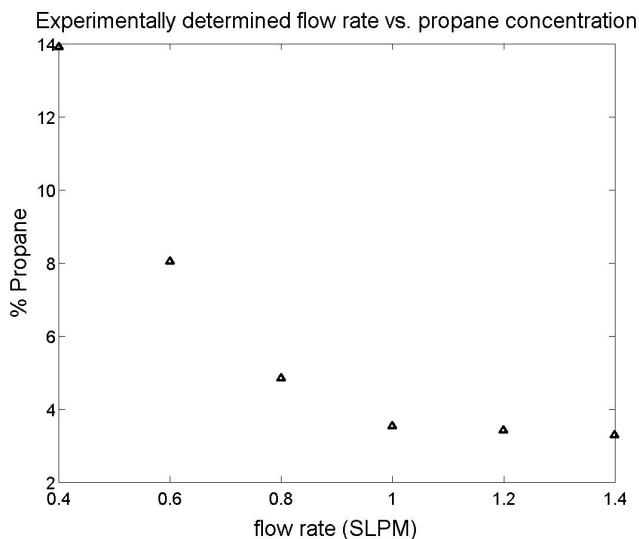
(b) Volumetric flow rate vs. extinction concentration: propane

Figure 3.8. Experimentally determined plot of volumetric flow rate versus extinction concentration of fuel (methane or propane) when fuel is convecting. Here the flow rate (top tube array) for oxidizer is $m_o = 1.8$ slpm for methane and $m_o = 1.9$ slpm for propane and the concentration of oxygen is 100% for methane and 80% for propane. Note that for high flow rates at the porous plate, the extinction appears to asymptote to a constant value and these extinctions are stable.

For both methane and propane with fuel convecting (see Figure 3.9), a fuel rich branch is less affected by a low flow rate change and more affected by a high flow rate change; whereas on the fuel lean side, the extinction concentration is more affected by low flow rates than high ones. Figure 3.9(b) shows experimental results on extinction concentrations for five different volumetric flow rates where propane is the fuels. When the oxidizer is held constant at 80%, an increase from $m_f = 0.4$ to $m_f = 0.6$ leads to a large difference (over 6%) in extinction concentration whereas an increase from $m_f = 1.0$ to $m_f = 1.2$ results in a much smaller change (less than 0.5%). While not as pronounced, there is a similar trend when the fuel concentration is held steady at 10%, but the lower flow rates exhibit a less pronounced difference. This sensitivity to the volumetric flow rate at the porous plate is important to consider when selecting a value to be used as a concentration extinction limit. Each fuel also has regions where burning only occurs within a certain range of volumetric flow rate. For example, in the plot showing experimental data on methane with fuel convecting (see Figure 3.9(a)) it is not possible for a flame to burn at 30% oxidizer and 20% fuel if the fuel flow rate is 1.9 *slpm*. Only at the lower flow rates can the flame exist. As the flow rate is increased, the flame approaches the tubes, and there is interference from heat losses to the tube array. Increasing the flow rate further causes the flame to enter the tube array. Conversely, low flow rates on the fuel lean side will not support a flame. The flame is observed to fall down to the porous plate and either extinguish or burn on one corner of the porous plate. Both configurations (fuel convecting and oxidizer convecting) exhibit this phenomena (see Figures 3.9 and 3.10) with the flow rate from the porous plate (bottom of the apparatus) being a major influence on the extinction concentrations.
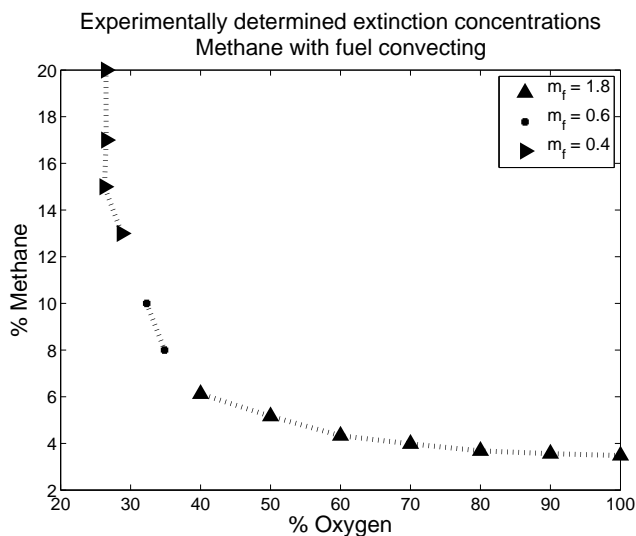
(a) Methane convecting
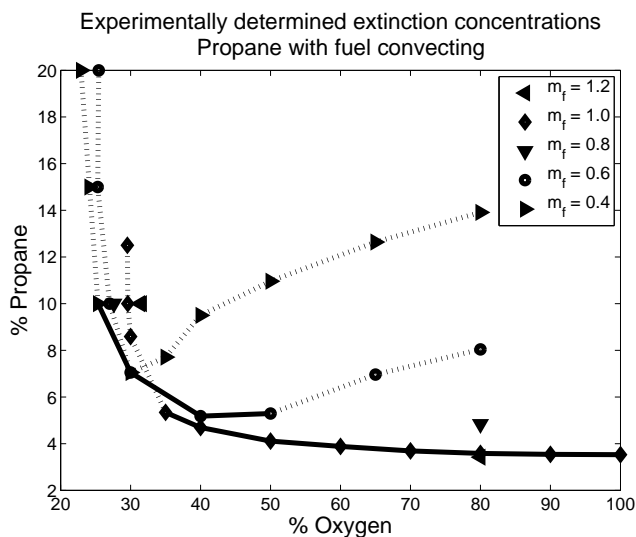
(b) Propane convecting

Figure 3.9. Experimental data: plot of concentration of fuel vs oxidizer for methane and propane with fuel convecting. The diffusing species (oxidizer) convects at 1.9 $slpm$. For methane (a), three different volumetric flow rates are shown and for propane (b), five different volumetric flow rates are shown with single points occuring for flow rates of $m_f = 0.8$ and $m_f = 1.2$ to show the effect of decreasing the flow rate on extinction concentration. Dotted lines indicate unstable flame extinction, solid lines indicate stable flame extinction.
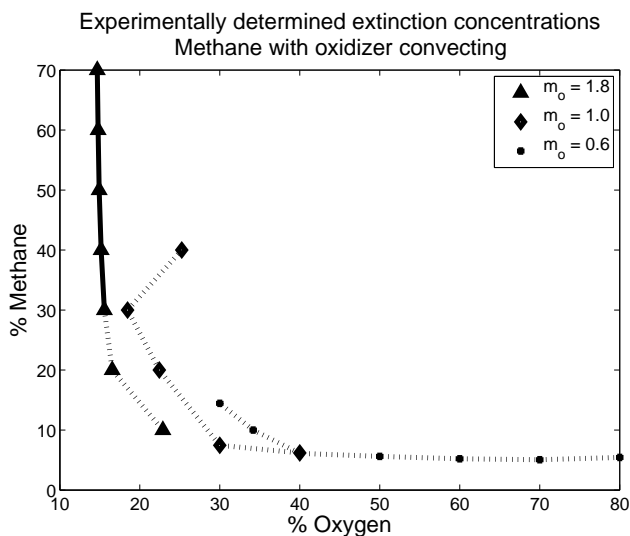
(a) Oxidizer convecting, methane
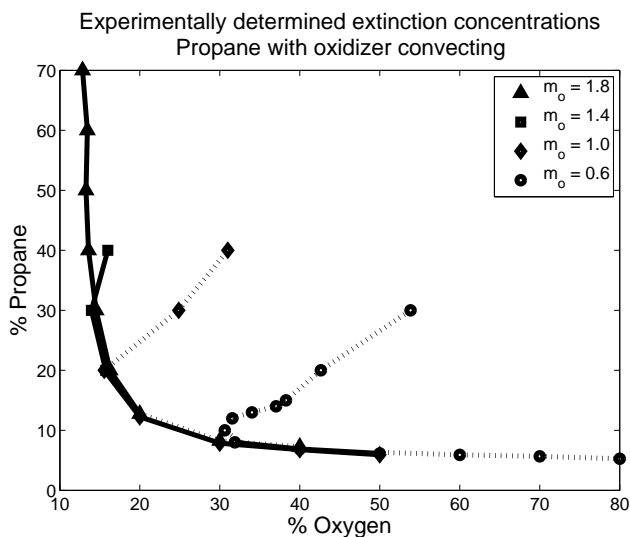
(b) Oxidizer convecting, propane

Figure 3.10. Experimental results: a plot of concentraion of fuel vs. oxidizer for methane and propane with oxidizer convecting. The diffusing species (fuel) convects at 1.9 $slpm$. For methane (a), three different volumetric flow rates are shown, and for propane (b) four different volumetric flow rates are shown. Dotted lines indicate unstable flame extinction, solid lines indicate stable flame extinction.

3.4.2. Comparison between Experimental and Numerical Results

While both numerical and experimental results show that the extinction concentration varies nonlinearly with mass flux, the overall trend in the numerics is different than that of the experiment. Compare the numerical plot (Figure 3.11) with the experimental plot (Figure 3.8(a)). As previously discussed, the experimental work (Figure 3.8(a)) has a linear zone where the extinction concentration is fairly constant over a range of different volumetric flow rates. Past a certain point (here, $m_f = 1.2 \ slpm$), the extinction concentration increases sharply. This same trend is not found in numerical simulations. Figure 3.11 shows a similar plot of extinction concentration vs mass flux (note here mass flux is in $\frac{kg}{m^2 sec}$). Instead of being a uniformly constant value, the numerical results indicate that the extinction concentration varies linearly with mass flux for mass fluxes greater than a certain critical flux and lower than this critical value (here $m = 0.003 \frac{kg}{m^2 sec}$) there is a sharp increase in extinction concentration values[8]. This behavior is found on both the fuel rich and fuel lean sides of the curves. Differences could be a result of heat loss in the experimental system that are not accounted for in the numerical model.

3.5. Unstable Behavior

Obtaining extinction data in planar flames can often prove difficult because instabilities can occur which in turn leads to early extinction. The thermal effects of colliding planar flames will be discussed in detail in the next chapter on flame holes (flame disks are a similar case). While the two systems are different in their setup (counterdiffusion flames versus counterflow flames), the general insight can be applied here. Understanding when

---

[8]Interestingly, there is no appreciable change in the behavior of the temperature at this critical mass flux.
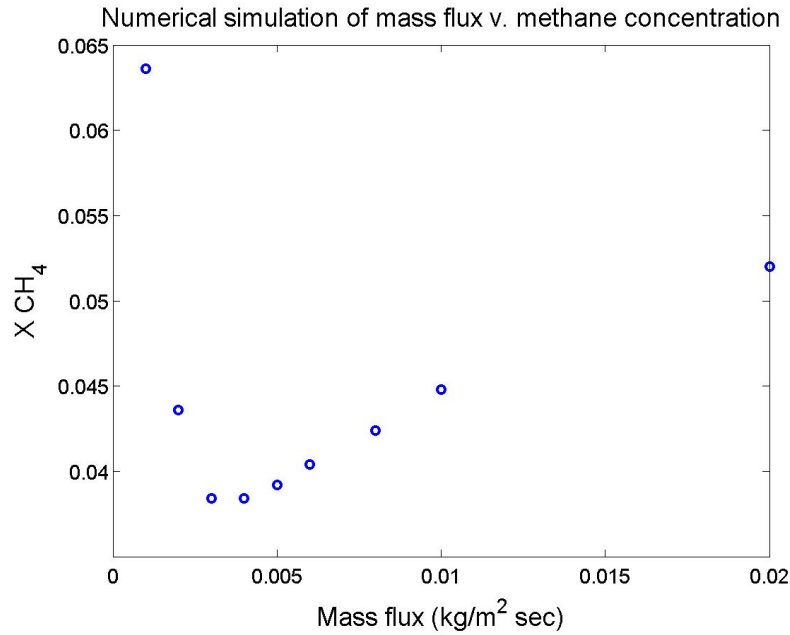
Figure 3.11. Numerical data for mass flux vs extinction concentration of fuel. Here the concentration of oxidizer was held constant at 90%

the onset of these oscillations occurs allows us to gain insight into the dynamics behind the instabilities as well as understand where the deficiencies in the calculated extinction curve occur and why. For this reason, we present a brief introductory look at instabilities that occur in the PPCD burner and set forth a new method of describing the different phenomena that occur.

3.5.1. Previous work

As discussed in the introduction, work by Matalon, *et al.* ([**49**] [**50**], [**53**], [**60**]) predicts cellular structures or oscillating behavior as the flame approaches extinction conditions. Experiments in a strained flame such as those conducted by Shay and Ronney [**39**] found no such cellular structure, due perhaps to the opposed, angled jets in their configuration resulting in a finite strain present in the system. Recently, Lo Jacono, *et al.* ([**51,**

56]) reported observations of a region of cellular instability near the extinction limit for CO_2 diluted H_2/O_2 systems consistant with the earlier findings of Matalon, *et al.* These instabilities occur as the flame sheet breaks into individual circular cells that then grow smaller before extinguishing. In addition, the individual cells have some horizontal translation (in the plane of the flames).

3.5.2. Observed Instabilities

The instabilities that were observed were most likely related to Rayleigh-Benard type instabilities, thermo-diffusive type instability, or a combination of both. In general, seven different types of oscillations were observed for methane-oxidizer systems and propane-oxidizer systems and are presented in table 3.5. Some are actually subsets or onsets of others, but to be consistent, all the different types were recorded and relationships between them noted. Instabilities seem to be consistent between propane and methane cases with the same types of oscillations occurring in each. While some were observed more frequently, lack of observation of a type of oscillation could simply imply that the region where it is common was not explored in depth. No cellular formations similar to the H_2/O_2 case were observed for either fuel under any conditions. The onset of these oscillations marks a higher extinction concentration than that of a stable flame due to strong perturbations in such oscillations. Under certain conditions (usually very low flow rates when fuel is convecting), the flame will fall to the bottom and burn there. These flames are not counted in either extinction cases or in the oscillations as they cannot be said to have extinguished.

While proximity to the tubes can be a factor in the onset of oscillations, it is not the only factor to be considered. Often with the oxidizer convecting, for low oxidizer flow rates, the flame is well away from the tubes (0.5 cm or more) when oscillations are observed since the Rayleigh number increases as the flame moves away from the tubes. Lo Jacono [56] showed that, in the PPCD burner when hydrogen and oxygen are burning, the Rayleigh number increases from around 240 when the flame is at distance of 4 mm from the tubes to near 800 when the flame is 6 mm from the tube. Nield [61] gives a formula for calculating the critical Rayleigh numbers based on Prandtl number, and reports critical Rayleigh numbers for the onset of instability ranging from 320 to 1452 depending on the boundary conditions. This gives rise to the possibility that in addition to the thermo-diffusive type instabilities observed by LoJacono, et $al.$ [51], oscillations are potentially thermo-convective instabilities. Oscillations also occur in the fuel convecting case when there are low fuel flow rates. In both cases, the flames tend to exhibit instabilities that are out of the plane of the flame such as type 1, 2, 4 or 7. The other instabilities do seem to occur more when the flames are near the tubes. Type 5 instabilities can occur away from the tubes, but are observed primarily near the tubes.

3.5.3. Results

3.5.3.1. Propane and Oxidizer with Oxidizer Convecting. For propane, when oxidizer is convecting, the oscillations have the effect of greatly increasing the extinction concentration of fuel (see Figure 3.9(b)). The flames are constant with no oscillations for large concentrations of oxidizer (fuel lean) when fuel is decreased to extinction up

Table 3.2. Descriptions of different types of observed flame instabilities

(1) Cat Tongue: One side of the flame flickers–slow down, fast up. This type starts out affecting only the side it is on; however, as it increases in amplitude affects the rest of the flame first spatially shifting it then causing a wave to move through the flame. (See Figure 3.12)

(2) Licking Dog: Similar to cat tongue but more periodic. It tends to stay more confined with faster oscillation, but it is similar to the previous in its development. Often this manifest as tongues on both sides of the flames flicking either in tandem or opposite. (See Figure 3.13)

(3) Shrinking Flame: Flame appears to shrink and grow always in the plane of the flame. Pulsations can come and go when first observed. (See Figure 3.14)

(4) M-flame: related to the cat tongue and licking dog, however, the oscillations cause the flame to become M-shaped with flickers on both side (either of type 1 or 2). As this progresses, it appears as though it is originating from one point (becoming more of an A-frame). (See Figure 3.15)

(5) Roach Flame: Flame shrinks to be a small (approximately one centimeter flame) before flashing back and forth rapidly. (See Figure 3.16)

(6) Magician's Flame: Flickers on the left before winking out leaving a small (approximately one centimeter) flame on the right. This generally stays steady but sometimes leads to a roach flame before extinguishing. (See Figure 3.17)

(7) Lightening Flame: Starts with a type 2 oscillation with tongues on either side, then as it progresses it tends to shrink to one side. As it does, it will flash out and down to the other side. After the flash, the shortened flame is on the other side and the process repeats. (See Figure 3.18)

to a certain point. At a critical concentration level of fuel, the oscillation frequency increases again. This leads to a case where if the system is started in the vicinity of the critical value, extinction can be caused by either increasing or decreasing the fuel concentration. If the fuel is increased, oscillations slowly set in, then grow to the point where they extinguish the flame. When the fuel is decreased, no oscillations are observed near extinction. The critical fuel concentration can be increased by increasing the oxidizer flow rate. For example, when the oxidizer flow rate is 0.6 $slpm$, the minimum fuel extinction concentration that can be obtained is around 10%; however, when the oxidizer flow rate is increased to 1.0 $slpm$, the minimum fuel concentration that can be obtained is closer

Conditions Under Which Oscillations Occur

Type	Convecting Species	Convecting Species Vol. Flow Rate (slpm)	Extinction	
			Fuel %	Oxidizer %
1.	CH_4	0.6-0.9	17.76	100
	C_3H_8	0.4	7.71	35
	O_2 (in C_3H_8)	0.6	8-20	31.88-44.02
2.	CH_4	1.1-1.2	9.76	100
	C_3H_8	0.4, 0.6	9.47, 6.96	40, 65
3.	CH_4	1.3-1.5	7.68	100
	O_2 (in CH_4)	1.8	20	16.55
	O_2 (in C_3H_8)	1.8	60, 70	13.52,12.84
4.	C_3H_8	0.4, 0.8	9.47 4.84	40-80
5.	CH_4	0.4-1.7	8-20	26.57-44.88
	C_3H_8	0.4-0.6	8.59-20	22.91-30
	O_2 (in CH_4)	0.6	5.44- 6.11	40-80
6.	CH_4	1.8	3.48-5.16	50-100
	CH_4	0.4	15	26.28-29.49
	O_2 (in CH_4)	0.6	5.05-5.44	60-80
	O_2 (in C_3H_8)	0.6	20-60	5.37-12.74
	O_2 (in C_3H_8)	1.0	20-40	6.78-12.25
7.	C_3H_8	0.4	12.64-13.91	65-80
	O_2 (in CH_4)	1.0, 0.6	40, 10	25, 34.17
	O_2 (in C_3H_8)	0.6	20	44.02

Table 3.3. Sample conditions under which each instability type was observed are documented with the extinction percentages indicated. For each case, assume the diffusing species (from the tube) has a flow rate of 1.9 slpm, unless indicated. Methane is CH_4, propane is C_3H_8, and oxygen is O_2.

to 20%. An oxidizer flow rate of 1.8 *slpm* shows hardly any oscillations, though higher oxygen concentrations exhibit higher propane extinction concentrations creating a slight bend in the curve. This could indicate that perhaps a minimum has been reached; but, the curve does not extend high enough to exhibit the oscillations observed for lower flow rates.

When burning on the fuel lean side, there is a clear delineation between stable and unstable flames. Below a certain fuel concentration, the flames can be stepped to extinction without oscillations. On the fuel lean side, the most common method of extinction is a type 6 instability, but this can still be considered an extinction of a laminar planar flame because while there is some oscillations before the flame shrinks, once it is small it goes to extinction the same way as the larger flames. Once the fuel level is above a certain value, decreasing the oxidizer leads to the extinction of flames at a higher oxidizer concentration than lower flow rates. This phenomenon leads to a curve that has extinction points for two different fuel concentrations. A quick study shows that this is indeed the case. By starting at an intermediate value and decreasing the fuel, extinction can be reached. Conversely, at the same starting point, by increasing the fuel, oscillations begin to occur and finally the flame extinguishes. The onset of the instability seems to correlate with the turning point of the curve. Again, it is possible to get partial extinction when the flame settles down to the bottom after a type 4 instability.

3.5.3.2. Propane and Oxidizer with Fuel Convecting. Similar to the case where oxidizer convects, there are different extinction curves for different flow rates. When fuel is convecting, it was not possible to stabilize the flame for large fuel concentrations, independent of flow rate. For example a fuel concentration of 20% was unstable for a variety of oxidizer concentrations and fuel and oxidizer flow rates. It was possible to change the type of oscillation, but, it was not possible to eliminate the oscillation completely. Fuel flow rates as low as 0.2 *slpm* and as high as 0.8 *slpm* (where the flame was causing the tubes to glow) were tried. Type 1 oscillations were observed for low flow rates, while type 5 oscillations were observed for larger flow rates. Stable flames were observed on the fuel

lean side of the curve for large flow rates. For smaller flow rates, instabilities of types 5, 2, and 7 were observed. Similar to the oxidizer cases, there were regions where two different oxidizer concentrations can be found for one fuel concentration when smaller flow rates are used. The effect is more pronounced as higher oxidizer concentrations are used.

With fuel convecting through at 20% fuel, different combinations of oxygen concentration and flow rates failed to yield a stable flame close to extinction. It was possible to change the types of instabilities. The most common instability for these flames were type 5, type 2 and type 1 instabilities, and at very low fuel flow rates, even type 4 (see section 3.5 for further details on instabilities). When running cases such as $m_o = 1.9$ $slpm$, $m_f = 0.6$ $slpm$, and fuel concentration of 10%, extinction concentration of oxygen cannot be determined because a type 4 instability leads to the flame falling to the bottom of the apparatus.

3.5.3.3. Comparisons between methane and propane. While methane exhibits the same behavior as propane, the methane flame is much less stable than the propane flame. Comparison between the fuel convecting plots (Figure 3.9) shows the difficulty of isolating a stable flame in the case with methane over that with propane. It was observed that it is possible to map the propane curve for a wider range of flow rates than was possible with the methane. It is possible that the Lewis number may be an indicator of the type of oscillations that would be observed; but, further research would have to be done to corroborate this.

For both methane and propane, the case where the oxidizer was convecting proved to be a more stable configuration where nearly the entire extinction curve could be successfully mapped (compare the oxidizer convecting curves Figure 3.10 with the fuel convecting

curves Figure 3.9). When fuel was convecting, it was difficult to find a steady flame as the concentration of fuel increased. For methane, this effect was greatly increased to the point where it was nearly impossible to get a true stable extinction curve for the fuel convecting case. In this configuration, using the maximum possible flow rate for the oxidizer, it was difficult to keep the flame out of the tubes. Interestingly, when fuel was convecting through the tubes, the flame extinguished at a lower concentration of methane than when the oxidizer was convecting when the system was fuel lean *i.e.* on the oxidizer size of the curve (see Figure 3.4). On the fuel rich side of the curve, the case where the oxidizer convects through extinguished at a lower concentration of oxygen than did the case where the fuel was convecting through. The cross over point appears to be around 10% fuel, 25% oxygen for propane and 6% fuel and 40% oxygen for methane.

3.6. Conclusion

Experimentally and numerically determined limiting extinction curves for propane and methane were presented with a comparison between the behaviors exhibited in both. The difficulty of analyzing the fuel rich side of the curve was discussed and used to explain the lack of data from the experimental results and the bending away from the asymptotic limit expected from the numerical results. Numerically, simulations using one step reactions were compared with complex chemistry models showing how both exhibit the same behavior and validating the use of the one-step reaction assumption used in the related theoretical models.

Through these investigations a better understanding of how mass flux affects extinction was explored, showing for different regions of the extinction curve, different mass fluxes
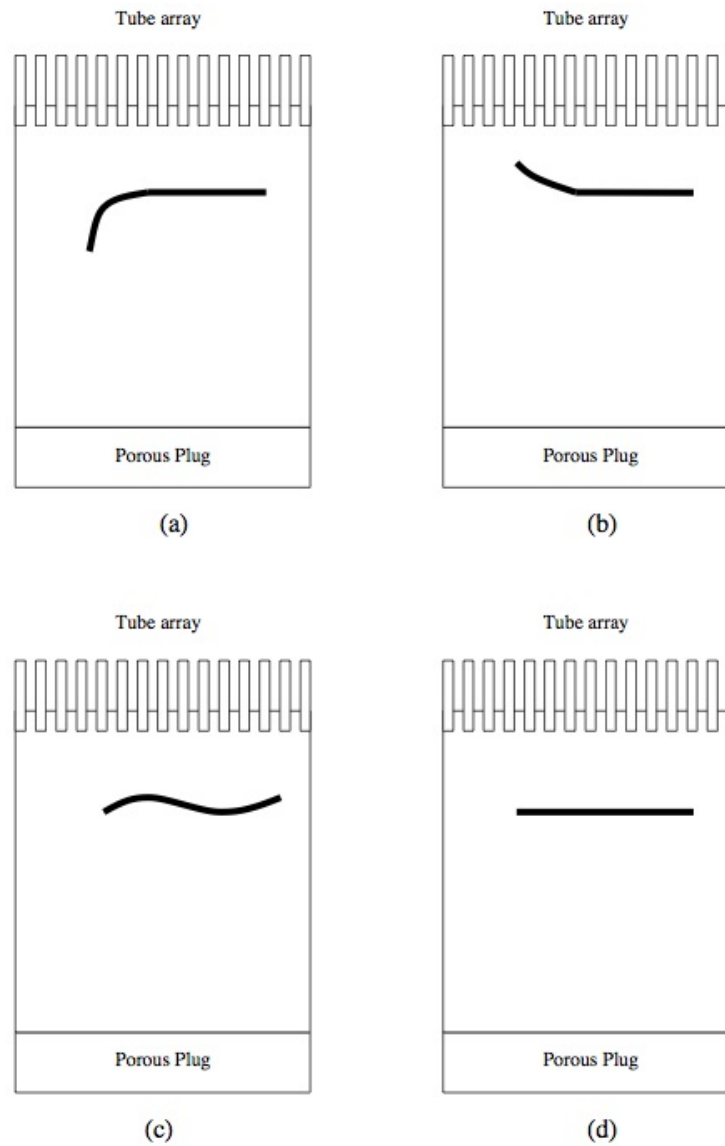
Figure 3.12. Cat tongue: Type 1 oscillation (side view of the burner). Figure (a) shows the beginning of the oscillation where the flame licks down slowly out of the plane of the flame. In mild oscillations, it will go between this state and the flat flame (Figure (d)). Once the oscillations start to increase in amplitude (which often is coupled with an increase in frequency), it will go from (a) to (b), where it has flicked up quickly. As the oscillations grow, the flame plane itself will start to be disturbed (Figure (c)) and then it returns to the stable state (Figure (d)).
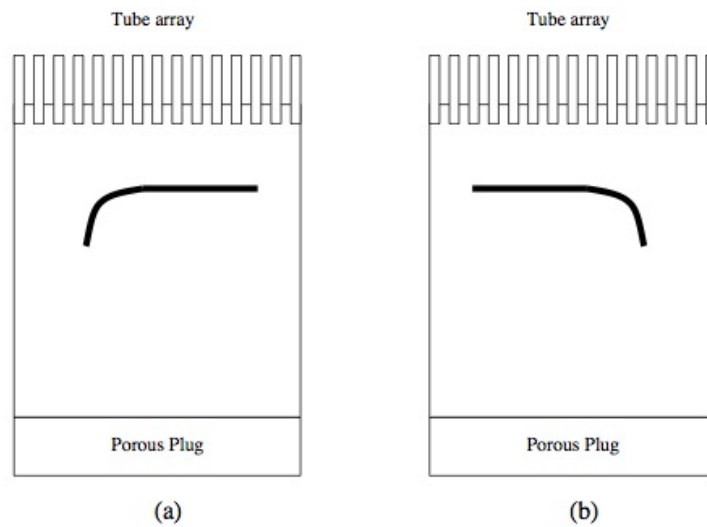
Figure 3.13. Licking dog: Type 2 oscillation (side view of the burner). Similar to the type 1 oscillation, the flame dips out of the plane of the flame (as shown in Figure (a)). This time, the oscillations occur with more regularity, and can occur on either or both sides of the flame (and will often go from one side to the other).
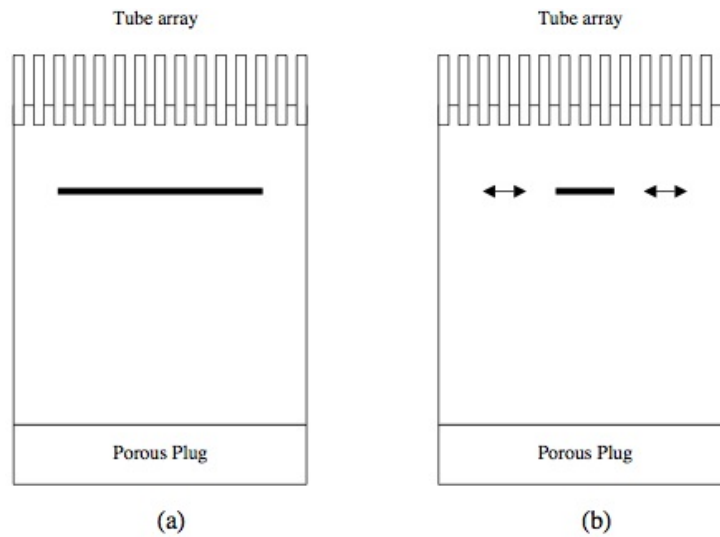
Figure 3.14. Shrinking flame: Type 3 oscillation (side view of the burner). Oscillations occur when the flame shrinks and expands in the plane of the flame.
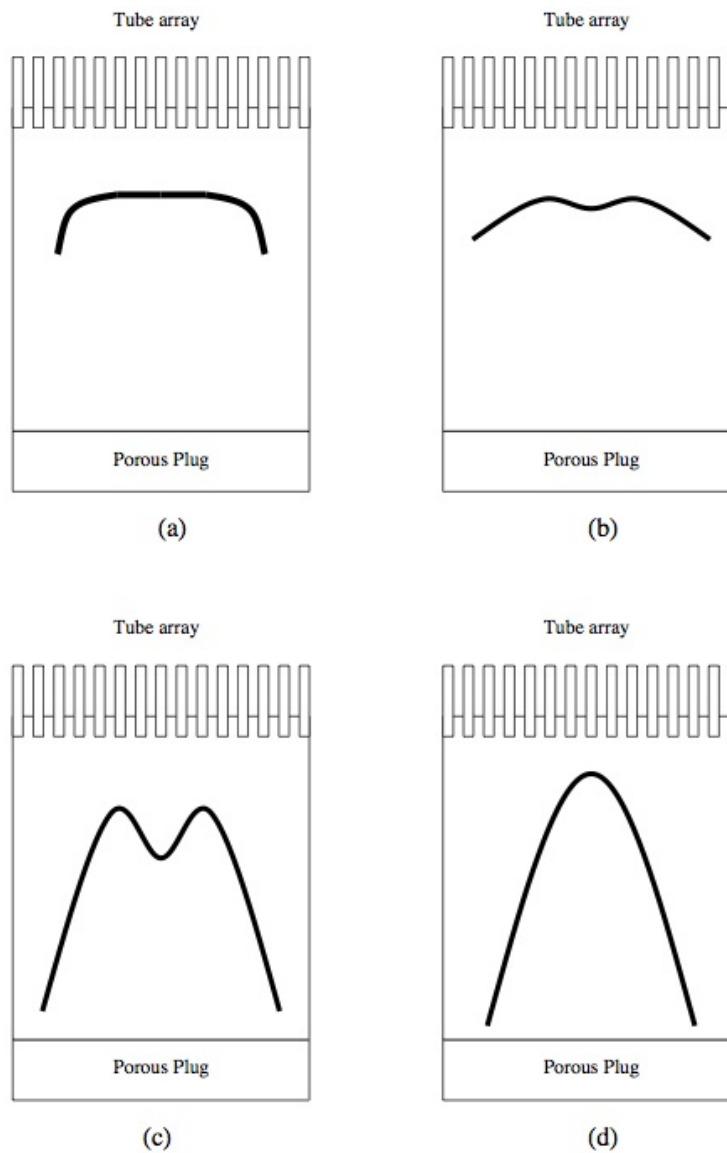
Figure 3.15. M-flame: Type 4 oscillation (side view of the burner). Oscillations begin like a type 1 or 2 oscillation with both sides moving together (a). As the amplitude grows, the flame plane takes on a warped m-shape with distinct peaks (b). The oscillations here can lead to extinction or the tails of the M can anchor onto the bottom burner (c) and eventually this looks like a single point (A-frame shape) (d).
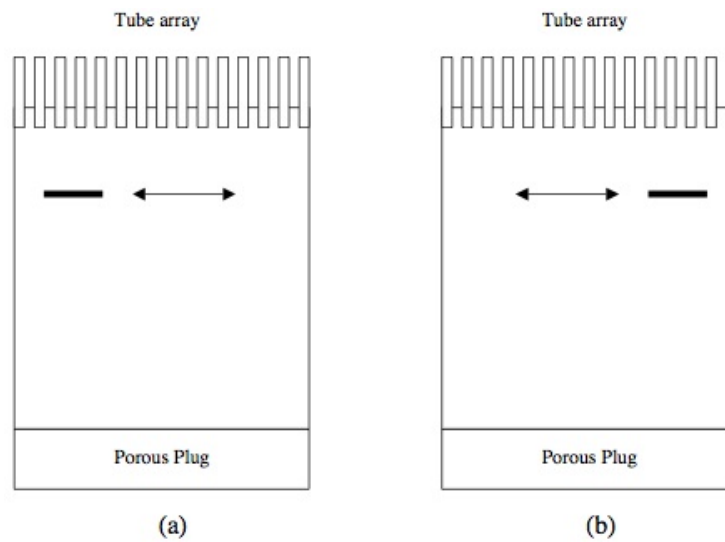
Figure 3.16. Roach flame: Type 5 oscillation (side view of the burner). Oscillations occur when the flame shrinks to a small disk, then oscillates back and forth in the plane of the flame.
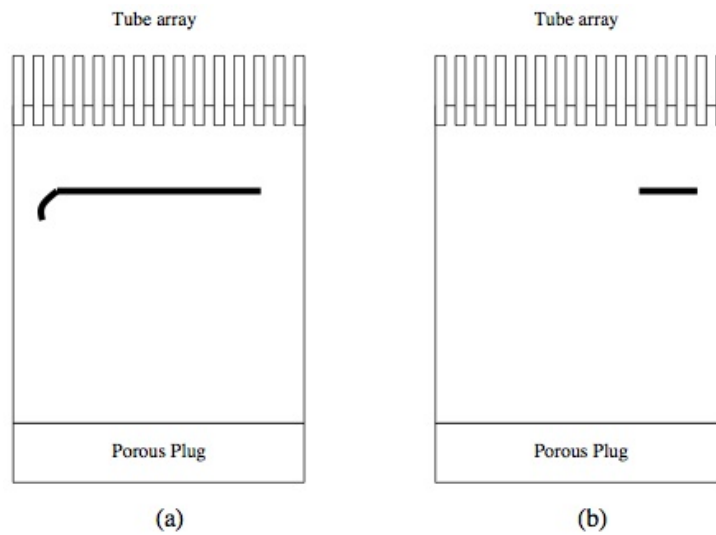
Figure 3.17. Magician's flame: Type 6 oscillation (side view of the burner). Oscillations start off with a small flicker on the left then the flame winks out leaving a small flame on the right. This occasionally stays steady before extinguishing , but sometimes leads to a type 5 instability before extinguishing.
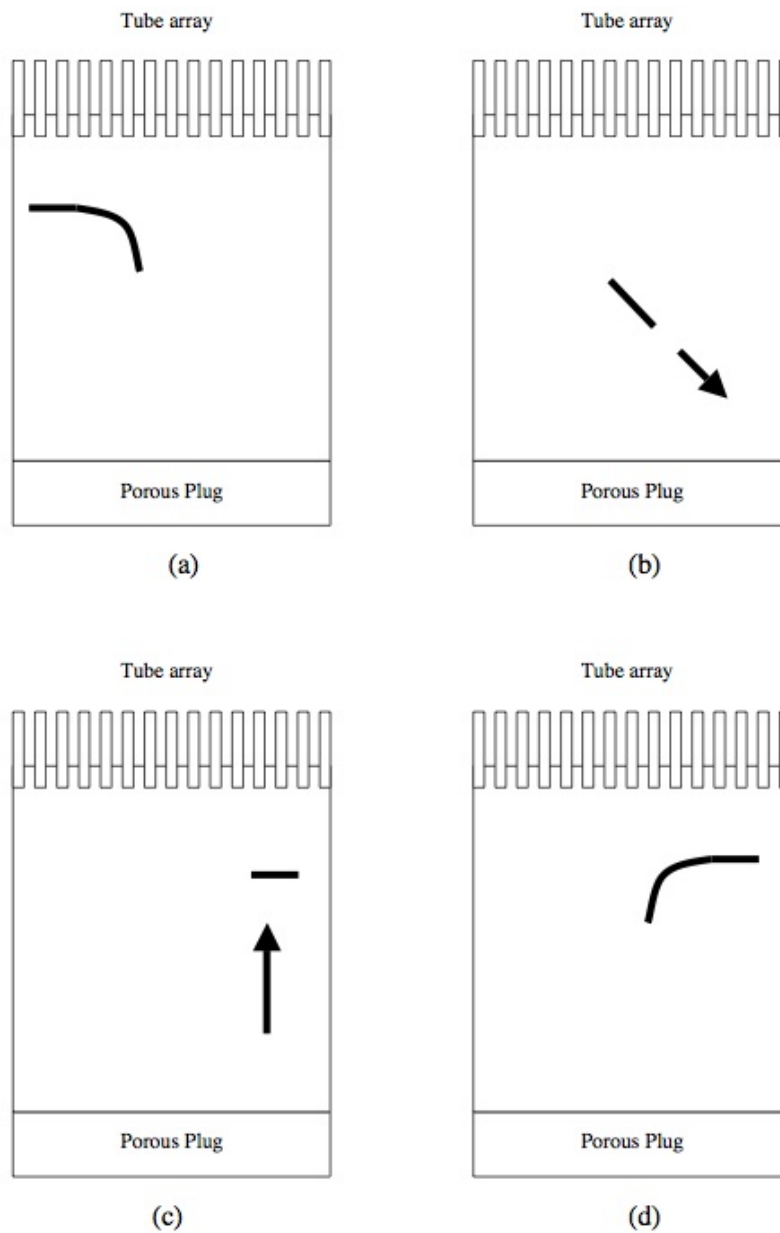
Figure 3.18. Lightening flame: Type 7 oscillation (side view of burner). Flame starts as a small disk, laps out like the start of a type 1 instability (a), flame flashes down to the opposite corner of the burner (b), then reestablishes itself as a flame disk (c) before repeating in the opposite direction (d).

are optimal. If a mass flux is too large, the flame is blown into the tubes and to small then oscillations occur. Given different flow rates, various regions where burning was and was not possible were explored. Since extinction curves might be a composite of two or three different mass fluxes, this work helps in providing understanding as to why and how those curves are chosen. Future work could include investigations of the influence of the mass flux through the tube array, as practically that is also an important factor in delivering the diffusive species to the flame plane; however, a full exploration of parameter space for both top and bottom flow rates will require a very extensive survey.

A preliminary examination of the types of oscillations observed for different regions of the fuel/oxidizer extinction curve and for different mass fluxes was conducted. It was found that the instabilities that occurred for methane and propane flames were categorically different than those observed in hydrogen flames. The methane and propane flame instabilities described here tended to be oscillatory in nature with the flame plane either deforming or shrinking, but remaining undivided. For low Lewis number fuels, the thermo-diffusive instability for relatively low Lewis number flames breaks the flame plane into smaller cells but it is possible that the thermo-diffusive instability is manifested as oscillations of the type describe here. The onset and behavior of the propane and methane cases were discussed for both fuel convecting and oxidizer flowing. Comparing methane and propane, it was discovered that propane was more stable, and therefore we expect the extinction curves determined to be more accurate. Future work would incorporate a wider analysis of the instabilities that occur, and perhaps numerical work that is being done with three dimensional fluid flows will allow a better understanding of how the fluid dynamics near the tube arrays influences the oscillations. This preliminary work sets

the groundwork for a wider look into unstable behavior, providing a framework wherein a more comprehensive investigation including video documentation of the flames can be conducted to establish the true range of flame instabilities. This work should be coupled with analytical work to provide further understanding as to why different instabilities occur.

CHAPTER 4

The Effects of Lewis Number on the Collapse of Holes in Planar Flames

4.1. Introduction

This work will focus on understanding the effects of Lewis number and strain rate on the collapse of flame holes. Equations will be developed in Section 4.2.1 with numerics discussed in Section 4.2.2. Results will be discussed in Section 4.3. Next, we examine the relationship between the collapse rate of flame holes and Lewis number and derive some emperical scaling laws for the dependence of hole radius on various parameters. The effect of Lewis number on critical radius also will be discussed.

4.2. Formulation of the Problem

To model flame dynamics, it is necessary to consider transport of species and temperature together with the dynamics of the fluids. The equations governing the system are the general conservation equations for multi-component, reacting, ideal gas mixtures, including the equations for continuity, momentum conservation, energy conservation, and conservation of species (Williams [9]). Various simplifying assumptions are needed to create a tractable problem including, ignoring the Soret[1] and Dufour[2] effects, body forces,

---

[1]The Soret effect, also called thermophoresis, is the effect of moledules drifting along temperature gradients [62].

[2]The Dofour effect is "if temperature gradients give rise to diffusion velocities (thermal diffusion), then concentration gradients must produce a heat flux" [9].

bulk viscosity, radiant heat flux, and assuming steady[3], low speed flow[4]. The fundamental equations incorporating these assumptions are commonly known as the Shvab-Zeldovich formulation. Moreover, we consider only a one-step reaction between fuel (denoted with the subscript f) and oxidizer (denoted with the subscript o).

4.2.1. Relevant Equations

Following the notations used in Lu [3] the species conservation considering convection, diffusion, and reaction can be written (for both fuel and oxidizer where the subscript i is either f or o for fuel or oxidizer, respectively) as:

$$(4.1) \qquad \frac{\mathrm{D}Y_i}{\mathrm{D}t} = D_i \nabla^2 Y_i - \frac{\nu_i m_i}{\rho}\omega$$

where ρ and the total derivative are in reference to the fluid, Y_i is the mass fraction of species i, D_i is the mass diffusivity, ν_i is the number of molecules of reacting, m_i is the molecular mass, and ω is the reaction rate in number of reactions in unit volume per unit time.

Conservation of energy requires (ignoring viscous dissipation and assuming the ideal gas law):

$$(4.2) \qquad \rho c_p \frac{\mathrm{D}T}{\mathrm{D}t} - \frac{\mathrm{D}p}{\mathrm{D}t} = k_T \nabla^2 T + Q\omega$$

---

[3]Steady state indicates there is no time dependence for the fluid flow. Note, this does not affect the time dependences of the concentration and the heat flux. It does, however, permit the integration of the continuity equation.

[4]This allows the assumption that the pressure is constant, thereby negating the need to separately consider the conservation equation.

where c_p is the specific heat at constant pressure for the fluid, T is the temperature, p is the pressure, k_T is the thermal conductivity, and Q is the amount of heat released per unit mass of the reactants consumed. By making the assumption that the gases behave as ideal gases and that there is low speed flow, therefore pressure drops are negligible, we can argue that the total derivative for pressure should be dropped such that the heat equation simplifies to:

$$(4.3) \qquad \frac{\mathrm{D}T}{\mathrm{D}t} = \frac{k_T}{\rho c_p} \nabla^2 T + \frac{Q}{\rho c_p} \omega$$

For the reaction rate, a global Arrhenius law is used:

$$(4.4) \qquad \omega = A \rho^{\nu_f + \nu_o} Y_f^{\nu_f} Y_o^{\nu_o} \exp\left(-\frac{T_a}{T}\right)$$

here A is the pre-exponential factor and T_a is the activation temperature ($T_a = \dfrac{E}{R}$ where E is the activation energy and R is the universal gas constant. The activation temperature is constant for a given reaction.). While A has a slight temperature dependence, here it is assumed to be constant for simplicity. The density is taken to be constant so the constant B can be used: $B = A\rho^{\nu_f + \nu_o}$.

While the collapse of flame holes are a three dimensional problem (see Figure 4.1), if the system is assumed to be axisymmetric the problem can be reduced to a two-dimensional case. Using a cylindrical coordinate system $(\tilde{r}, \tilde{\theta}, \tilde{z})$ with a counterflow[5] so the radial velocity is proportional to the radius, $\tilde{u}_r = a\tilde{r}$, and the axial velocity is proportional to the distance from the flame plane and flows to the midplane: $\tilde{u}_z = -2a\tilde{z}$ and assuming symmetry about the radial direction (i.e. derivatives with respect to $\tilde{\theta}$ are

---

[5]Note this flow preserves continuity, $\nabla \cdot \vec{\mathbf{u}} = 0$
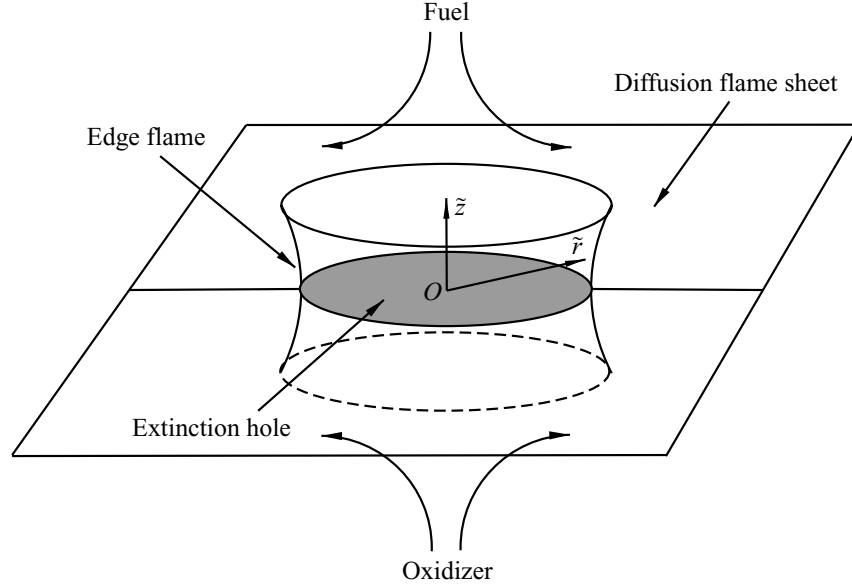
Figure 4.1. Three dimensional schematic of a flame hole with coordinate axes $(\tilde{r}, \tilde{\theta}, \tilde{z})$. Figure reproduced from Lu and Ghosal 2004 [43]

zero), equations 4.1 and 4.3 become (after dividing through by ρ):

$$(4.5) \qquad \frac{\partial Y_i}{\partial \tilde{t}} + a\tilde{r}\frac{\partial Y_i}{\partial \tilde{r}} - 2a\tilde{z}\frac{\partial Y_i}{\partial \tilde{z}} = D_i \left[\frac{1}{\tilde{r}}\frac{\partial}{\partial \tilde{r}}\left(\tilde{r}\frac{\partial Y_i}{\partial \tilde{r}} \right) + \frac{\partial^2 Y_i}{\partial \tilde{z}^2} \right] - \frac{\nu_i m_i}{\rho}\omega$$

and

$$(4.6) \qquad \frac{\partial T}{\partial \tilde{t}} + a\tilde{r}\frac{\partial T}{\partial \tilde{r}} - 2a\tilde{z}\frac{\partial T}{\partial \tilde{z}} = D_T \left[\frac{1}{\tilde{r}}\frac{\partial}{\partial \tilde{r}}\left(\tilde{r}\frac{\partial T}{\partial \tilde{r}} \right) + \frac{\partial^2 T}{\partial \tilde{z}^2} \right] + \frac{Q}{\rho c_p}\omega$$

where D_T is the thermal diffusivity defined as:

$$(4.7) \qquad D_T = \frac{k_T}{\rho c_p}.$$

In the far field, it is assumed that the temperature and the concentrations are constant:

$$(4.8) \qquad \frac{\partial}{\partial \tilde{r}} T(\infty, \tilde{z}, \tilde{t}) = \frac{\partial}{\partial \tilde{r}} Y_i(\infty, \tilde{z}, \tilde{t}) = 0.$$

Far from the flame plane (i.e. as $\tilde{z} \to \pm\infty$) the temperature returns to an unburned temperature:

$$(4.9) \qquad T(\tilde{r}, \pm\infty, \tilde{t}) \to T_u,$$

and both fuel and oxidizer asymptote to their unburned mass fractions on their respective sides of the flame plane and zero on the other.

$$(4.10) \qquad Y_o(\tilde{r}, -\infty, \tilde{t}) \to Y_{ou} \qquad Y_o(\tilde{r}, +\infty, \tilde{t}) \to 0$$

$$(4.11) \qquad Y_f(\tilde{r}, -\infty, \tilde{t}) \to 0 \qquad Y_f(\tilde{r}, +\infty, \tilde{t}) \to Y_{fu}.$$

Thus, logical non-dimensionalizations for the fuel, oxidizer, and temperature are:

$$(4.12) \qquad y_f = \frac{Y_f}{Y_{fu}} \qquad y_o = \frac{Y_o}{Y_{ou}} \qquad \theta = \frac{T - T_u}{T_s - T_u}$$

Here, T_s is the adiabatic flame temperature.[6] The the heat produced per reaction is:

$$(4.13) \qquad Q = c_p \left(\frac{\nu_o m_o}{Y_{ou}} + \frac{\nu_f m_f}{Y_{fu}} \right) (T_s - T_u).$$

---

[6]The temperature found at the flame plane under stoichiometric conditions.

The Zeldovich number[7] is:

$$(4.14) \qquad \beta = \frac{T_a(T_s - T_u)}{T_s^2}$$

To characterize the length and time scales, we use the characteristic velocity determined from the leading order term in the asymptotic expansion for planar premixed flame velocity (for unity Lewis numbers) as v_0:

$$(4.15) \qquad v_0^2 = \frac{2BD_T(\nu_f m_f)Y_{ou}}{\beta^3 \rho} \exp\left(-\frac{T_a}{T_s}\right)$$

Using this as a velocity scale, the length scales and time scale are:

$$(4.16) \qquad r = \frac{\tilde{r} v_0}{D_T} \qquad z = \frac{\tilde{z} v_0}{D_T} \qquad t = \frac{\tilde{t} v_0^2}{D_T}$$

The strain rate parameter is defined as:

$$\lambda = \frac{aD_T}{v_0^2}$$

The Lewis number for species (Le_o for oxidizer and Le_f for fuel) is:

$$(4.17) \qquad Le_o = \frac{D_T}{D_o} \qquad Le_f = \frac{D_T}{D_f}$$

With these non-dimensionalizations and constants and taking $m_f = m_o$ and $\nu_f = \nu_o$, equation 4.5 becomes (for both fuel and oxidizer) (as given by Lu [3]):

$$(4.18) \qquad \frac{\partial y_i}{\partial t} + \lambda r \frac{\partial y_i}{\partial r} - 2\lambda z \frac{\partial y_i}{\partial z} = \frac{1}{Le_i}\left[\frac{1}{r}\frac{\partial}{\partial r}\left(r\frac{\partial y_i}{\partial r}\right) + \frac{\partial^2 y_i}{\partial z^2}\right] - \frac{1}{2}\beta^3 y_o y_f e^{-\beta(1-\theta)}$$

---

[7]The Zeldovich number is a "measure of the sensitivity of the reaction rate to temperature." [1]

and the temperature equation (equation 4.6) is now:

$$(4.19) \qquad \frac{\partial \theta}{\partial t} + \lambda r \frac{\partial \theta}{\partial r} - 2\lambda z \frac{\partial \theta}{\partial z} = \frac{1}{r} \frac{\partial}{\partial r} \left(r \frac{\partial \theta}{\partial r} \right) + \frac{\partial^2 \theta}{\partial z^2} + \beta^3 y_o y_f e^{-\beta(1-\theta)}$$

The boundary conditions must also be non-dimensionalized. Equation 4.8 becomes:

$$(4.20) \qquad \frac{\partial \theta}{\partial r}\big|_{(\infty,z)} = \frac{\partial y_i}{\partial r}\big|_{(\infty,z)} = 0$$

and the equations for temperature, oxidizer, and fuel in the axial direction (equations 4.9, 4.10, and 4.11) become:

$$(4.21) \qquad \theta(r, \pm\infty) \to 0$$

$$(4.22) \qquad y_o(r, -\infty) \to 1 \qquad y_o(r, +\infty) \to 0$$

$$(4.23) \qquad y_f(r, -\infty) \to 0 \qquad y_f(r, +\infty) \to 1$$

This set of differential equations will be solved numerically using methods discussed in the next section. We will be primarily concerned with how the Lewis numbers and strain rate affect the solutions.

4.2.2. Numerical Methods

The temperature, fuel concentration, and oxidizer concentration equations are solved simultaneously using a sixth order spatial derivative scheme and a first order time derivative scheme. Because of the symmetry of the problem, only half the domain is modeled. The

collision occurs at the left boundary ($r = 0$), and then the domain is doubled for post processing (plotting, etc.). A uniform spatial discretization is used with $n_r = 400$ points and $n_z = 500$ with the length L of the domain being $L_r = 20$ and $L_z = 30$. This allows the edges of the domain to be far enough that they are not affected by the dynamics of the flame. A Zeldovich number $\beta = 16$ is used.

Boundary conditions are taken as follows. At the collision plane, the symmetry boundary condition allows us to use zero derivatives which is implemented numerically by setting the value of the dependent variable to be identical at the last two adjacent points on the grid. The top of the domain and the bottom should be far enough from the flame that the values of fuel, oxidizer, and temperature have reached their far field values, thus the boundaries are set to their steady state values at infinity (at the top $\theta = 0$, $y_o = 0$ and $y_f = 1$, at the bottom $\theta = 0$, $y_o = 1$ and $y_f = 0$) . At the right boundary, we expect that things are not changing in the radial direction, thus the last two adjacent points on the grid are set to be identical.

All simulations are initialized by using a unity Lewis number solution, then allowing the flame to burn to a steady solution. A "hole" of radius r_f is artificially placed in the burning solution by setting the temperature, fuel concentration and oxidizer concentration to their unburned values:

(4.24)
$$T(r, z) = 0 \qquad \text{for } r < r_f$$

(4.25)
$$y_f(r, z) = \frac{1}{2} \left(1 + erf \sqrt{\lambda Le_o} \right) \qquad \text{for } r < r_f$$

$$(4.26) \qquad y_o(r, z) = \frac{1}{2}\left(1 - erf\sqrt{\lambda Le_f}\right) \qquad \text{for } r < r_f$$

Initially, the hole expands as the artificially imposed boundary softens and the triple flame develops, but once the system has equilibrated, the hole with either expand or contract, depending on the radius in relation to the critical radius[8]. Following the work of Lu [3], we elect to define the flame edge location r_f as the point where the reaction rate ω is maximized along the flame plane.

In order to estimate a curve fit $v_i = ar_f^{-b}$ to the flame edge velocity calculated from the data[9], we use an least squares regression as described by Ramanathan [63]. Ideally, we have:

$$(4.27) \qquad v = ar_f^{-b}.$$

To find this, we wish to minimize sum of the squares of the residuals. We take the logarithm of both sides and estimate the equation as,

$$(4.28) \qquad \log v = \log a - b \cdot \log r_f + \varepsilon,$$

(let us define $\alpha = \log a$). Thus the residual:

$$(4.29) \qquad \varepsilon = \log v - \alpha + b \log r_f.$$

---

[8]The radius at which the hole is at an unstable equilibrium.
[9]Here, v is the lab frame velocity adjusted from the calculated velocity v_s by taking into account the effects of convection. More details are available in the results section.

Next, the estimated variance ($\hat{\sigma}$) is given by:

$$(4.30) \qquad \hat{\sigma}^2 = \frac{\sum \varepsilon^2}{n-1}$$

We can minimize this to find the parameters a (or α) and b that give us the best curve fit using a Matlab routine that calculates a matrix of the different parameters and extracts the lowest $\hat{\sigma}$. To find the error on these coefficients, if

$$(4.31) \qquad S_{xx} = \sum \left(\log r_f - mean \log(r_f) \right)^2,$$

the standard deviation on $\log a$ is given by:

$$(4.32) \qquad \hat{\sigma}_\alpha^2 = \frac{\hat{\sigma}^2 \sum (\log r)^2}{(n-1)S_{xx}}$$

the standard deviation on b is given by:

$$(4.33) \qquad \hat{\sigma}_b^2 = \frac{\varepsilon^2}{S_{xx}}$$

Thus the errors on α and b will be given with a 95% confidence interval or $2\hat{\sigma}_\alpha$ and $2\hat{\sigma}_b$, respectively.

4.3. Results

4.3.1. General Observations of the Effects of Lewis Number

During this numerical study, different strain rates were examined, ranging from $\lambda = 0.2$ to $\lambda = 0.001$. Special care was taken with $\lambda = 0.1, \lambda = 0.05$ and $\lambda = 0.01$ with flame collapse

studied for an effective Lewis number[10] ranging from $Le = 0.6$ to $Le = 1.5$. In all cases, the reaction rate and temperature increases with decreasing Lewis number. Table 4.3.1 shows the steady state temperature, reaction rate, and fuel and oxidizer concentrations in the middle of the domain[11]. In general, the smaller the Lewis number, the hotter the flame, the stronger the reaction rate, and the larger the flame zone. For smaller Lewis numbers, the oxidizer content on the fuel side is greater indicating that the reaction zone is larger which is allowing more fuel to transport further. Correspondingly, the fuel concentrations on the fuel side decrease with smaller Lewis numbers for the same reason. Since the oxidizer can transport further, more fuel is burned and thus, the flame is hotter and broader. Since the Lewis number is the ratio of thermal diffusivity to mass diffusivity, this makes sense: the species can diffuse further across the flame zone. Figure 4.2 shows an example of two collapsing flames with different Lewis number ($Le = 1.0$ and $Le = 1.5$) for the same times. Following Lu [3], the time at collision is $t = 0$ with the time before collapse taken to be negative and the time after collapse as positive. Notice how the flame front moves faster in the case with the smaller Lewis number. The flame isolas of high reaction rates described by Lu are smaller and dissipate more slowly in the larger Lewis number case.

4.3.2. Relationship between Hole Collapse Rate and Lewis Number

Previous works (c.f. [**3, 42, 41, 38**] *et al.*) have considered the influence of different parameters such as the Damköhler numberon the flame front speed v, and here, we will examine how the Lewis number and strain rate affect the edge flame speed. First, the

----

[10]The effective Lewis number is where the fuel and oxidizer Lewis numbers are equal

[11]Here middle refers to slightly above the mid-plane as zero does not naturally fall in the domain

Table of Calculated Steady State Values for Various Strain Rates and Lewis Numbers					
λ	Le	Reaction rate	Temperature	Fuel	Oxidizer
0.1	0.6	1.444	0.9346	0.0410	0.0244
	0.7	1.434	0.9343	0.0418	0.0239
	0.8	1.424	0.9340	0.0426	0.0234
	0.9	1.414	0.9338	0.0433	0.0229
	1.0	1.400	0.9331	0.0440	0.0226
	1.1	1.391	0.9329	0.0447	0.0222
	1.2	1.381	0.9326	0.0453	0.0218
	1.3	1.371	0.9324	0.0459	0.0214
	1.4	1.362	0.9322	0.0465	0.0211
	1.5	1.352	0.9319	0.0471	0.0208
0.05	0.6	0.981	0.9542	0.0289	0.0172
	0.7	0.975	0.9540	0.0295	0.0168
	0.8	0.963	0.9530	0.0301	0.0165
	0.9	0.962	0.9535	0.0305	0.0161
	1.0	0.952	0.9527	0.0310	0.0159
	1.1	0.945	0.9524	0.0315	0.0156
	1.2	0.940	0.9522	0.0320	0.0153
	1.3	0.939	0.9528	0.0323	0.0150
	1.4	0.933	0.9526	0.0327	0.0148
	1.5	0.923	0.9516	0.0332	0.0146
0.01	0.6	0.370	0.9771	0.0143	0.0090
	0.7	0.369	0.9774	0.0145	0.0088
	0.8	0.368	0.9774	0.0148	0.0087
	0.9	0.366	0.9771	0.0150	0.0085
	1.0	0.358	0.9746	0.0153	0.0085
	1.1	0.356	0.9744	0.0155	0.0084
	1.2	0.354	0.9741	0.0157	0.0083
	1.3	0.353	0.9739	0.0159	0.0082
	1.4	0.351	0.9737	0.0161	0.0081
	1.5	0.349	0.9735	0.0162	0.0080

Table 4.1. Steady flame parameters at the mid-plane (top side) for $\lambda = 0.1$, $\lambda = 0.05$, and $\lambda = 0.01$. Shown are reaction rate, temperature, fuel concentration and oxidizer concentrations (all non-dimensional).
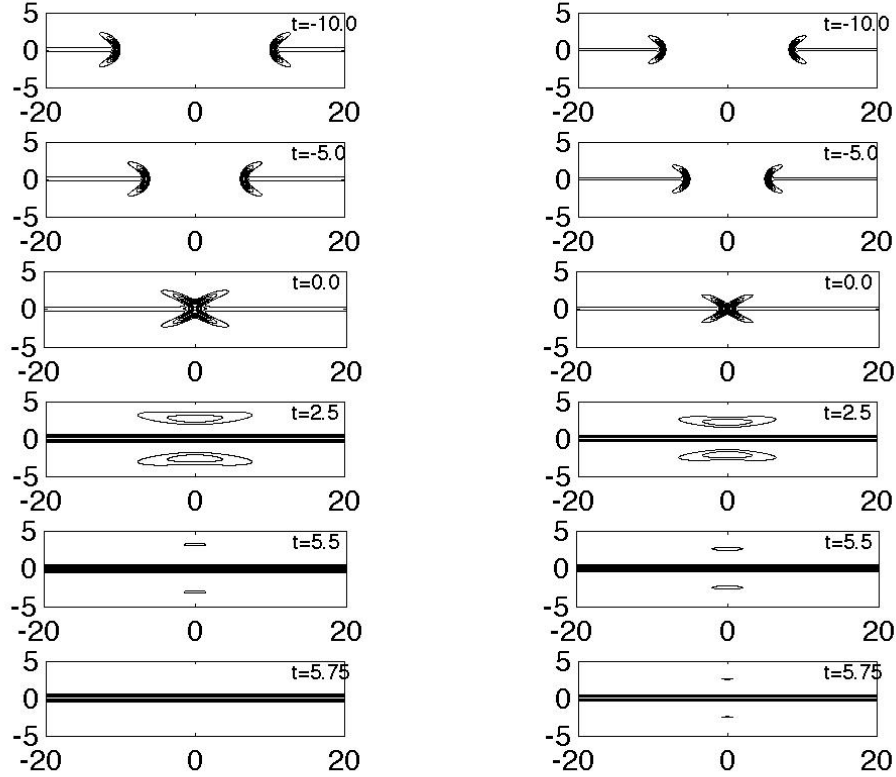
Figure 4.2. Temporal evolution of the reaction rate contours for two different Lewis numbers, $Le = 1.0$ on the left and $Le = 1.5$ on the right. Note how the lower Lewis number flame front travels at a faster speed. For the larger Lewis number, the isolas of high reaction rates are smaller and diffuse more slowly.

question of how to determine the flame position (and hence the flame speed) is a difficult one and has been pondered by Buckmaster and Jackson [41] and Lu [3] among others. Their convention is adopted, namely to use the peak of the reaction rate to track the "edge" of the flame and hence use that to calculate the edge flame velocity in the simulation (Figure 4.3 shows typical plots of edge flame vs time for different strain rates). Next, to consider the flame velocity, a coordinate transformation from the flame velocity

in the simulation v_s to the lab frame velocity (*i.e.* flame front speed as observed in from a stationary observer) is given by:

$$(4.34) \qquad\qquad\qquad v = v_s + \lambda r_f,$$

where λ is the strain rate (discussed previously) and r_f is the radius of the flame edge. Consistent with the results of Daou and Liñán [**38**], the flame speeds observed in the simulations drop with increasing Lewis number. Figure 4.4 gives resulting flame speed curves for various Lewis numbers (for strain rate $\lambda = 0.01$).

Plot of flame edge position vs. time for various strain rates
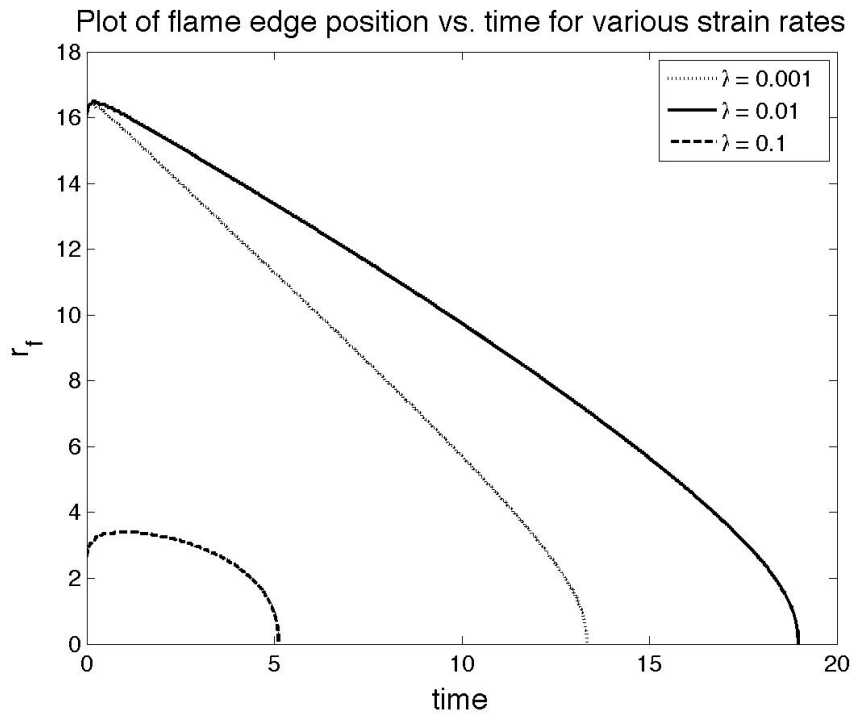
Figure 4.3. Plot of edge flame position vs time for various strain rates ($\lambda = 0.01$, $\lambda = 0.05$ and $\lambda = 0.1$). All cases are shown for $Le = 1.0$

Given previous results in the literature, if we look at the flame velocity near collision, we expect that since $r \propto t$, the curve for velocity will be related to radius through some
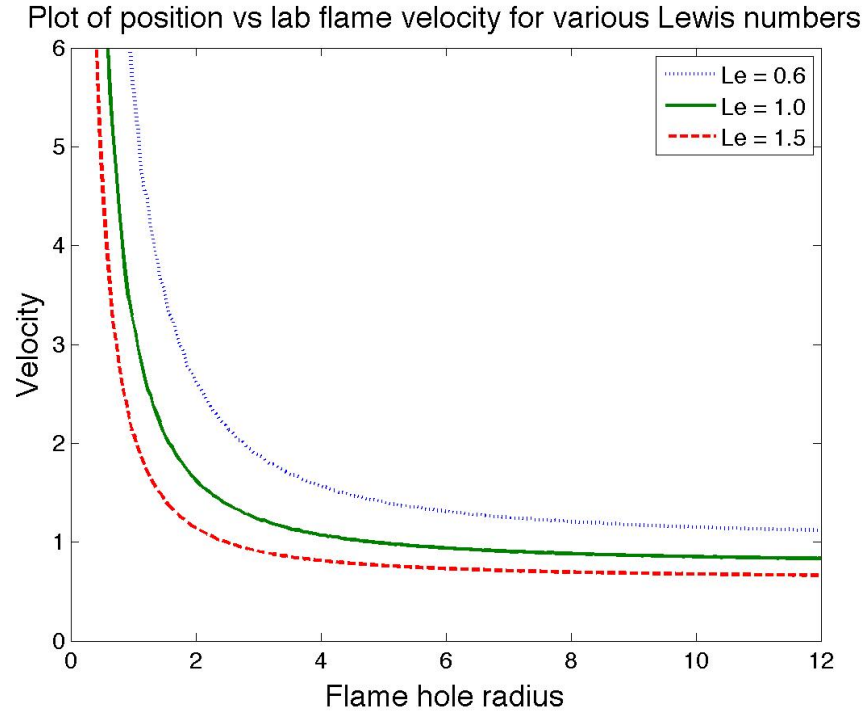
Figure 4.4. Shown here are the lab frame flame speeds for three different Lewis numbers. Note that, consistent with literature results, the flame's free stream velocity increases as the Lewis number decreases. The strain rate here is $\lambda = 0.01$.

polynomial expression of the form:

$$(4.35) \qquad\qquad\qquad v = a r_f^{-b}$$

where a and b are coefficients that are determined from the simulation results. For one-dimensional flame collapse with unity Lewis number, Lu [3] found the flame velocity to be:

$$v \sim \frac{\Lambda}{r_f}$$

where $\Lambda = 1.71$ is a numerically determined parameter. Pantano and Pullin [42] analytically determined the flame speed for a two dimensional unity Lewis number case of a

collapsing cylinder (limit of zero strain rate) as:

$$(4.36) \qquad v = \Lambda \left(\frac{1}{r_f} + \frac{2a}{\delta} \right)$$

where $\Lambda = 3.15991$ is a numerically determined eigenvalue, $a_2 = -0.262156$ is a parameter, and δ is a reduced Damköhler number. In the limit of large Damköhler number, this reduces to:

$$(4.37) \qquad v = \frac{3.15591}{r_f}$$

Using the numerical curve fitting described earlier where the final few points and the initial collapse are neglected, the values for a and b that minimize the sum of the squares of the errors are presented for different Lewis numbers and strain rates: Table 4.3 shows the value a, Table 4.4 shows the value of $\log a$, Table 4.5 shows the value b. For each Lewis number, a remains relatively constant, while for each strain rate b remains relatively constant. Our value for the coefficient a (their Λ) for $Le = 1.0$ of 3.4 is close to that of Pantano and Pullin, with the minor discrepancy due to numerical integration issues or curve fit estimations (it could also be due to their estimations and approximation of the system as a cylinder). Note, our value is nearly twice that predicted for planar flame collapse in the one dimensional case (by Lu), indicating the influence of the curved geometry has important effects on collapse. Interestingly, we find that the exponential coefficient, b depends strongly on strain rate. As the strain rate decreases, the value of the exponent approaches Pantano and Pullin's value of $b = 1$. Table 4.2 shows how the value of b increases with strain rate, Figure 4.5 shows how the value of b is nearly constant for a given strain rate, and Figure 4.6 shows how b varies with strain rate.

Values of b for various strain rates	
λ	$b \pm 2\sigma_b$
0.001	1.142 ± 0.008
0.005	1.155 ± 0.006
0.01	1.200 ± 0.007
0.03	1.235 ± 0.005
0.05	1.264 ± 0.006
0.08	1.367 ± 0.005
0.1	1.432 ± 0.005
0.15	1.644 ± 0.009

Table 4.2. Table of exponential b with a 95% confidence interval from the curve fit of velocity $(v = ar_f^{-b})$ for various strain rates. Values were taken by fitting the data to the simulation results. Data for $Le = 1.0$.
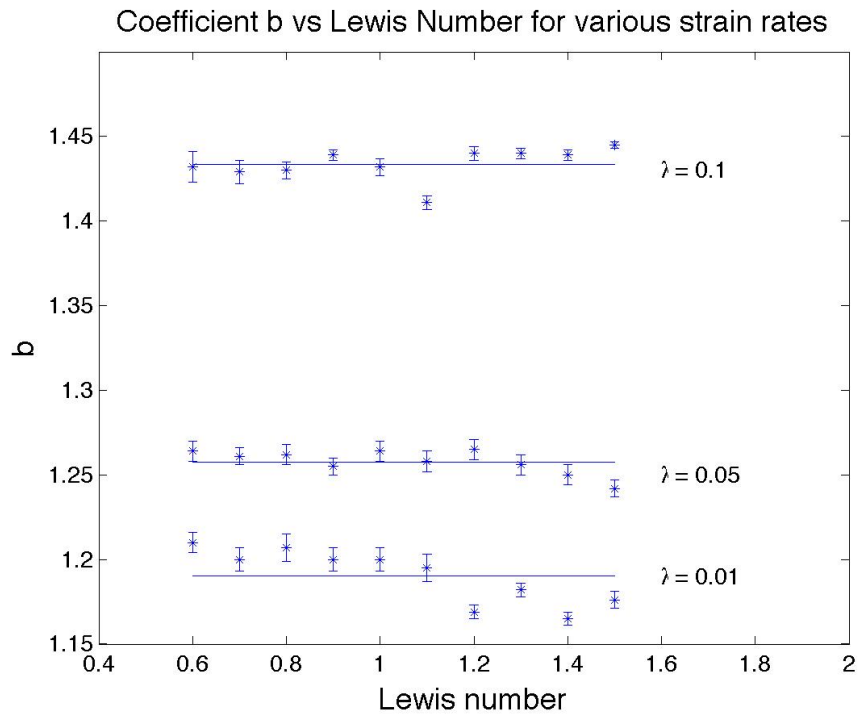
Figure 4.5. Plot of b versus Lewis number for $\lambda = 0.01$, $\lambda = 0.05$ and $\lambda = 0.1$. Here, the average values of b for a given strain rate are plotted as lines across the strain rate.
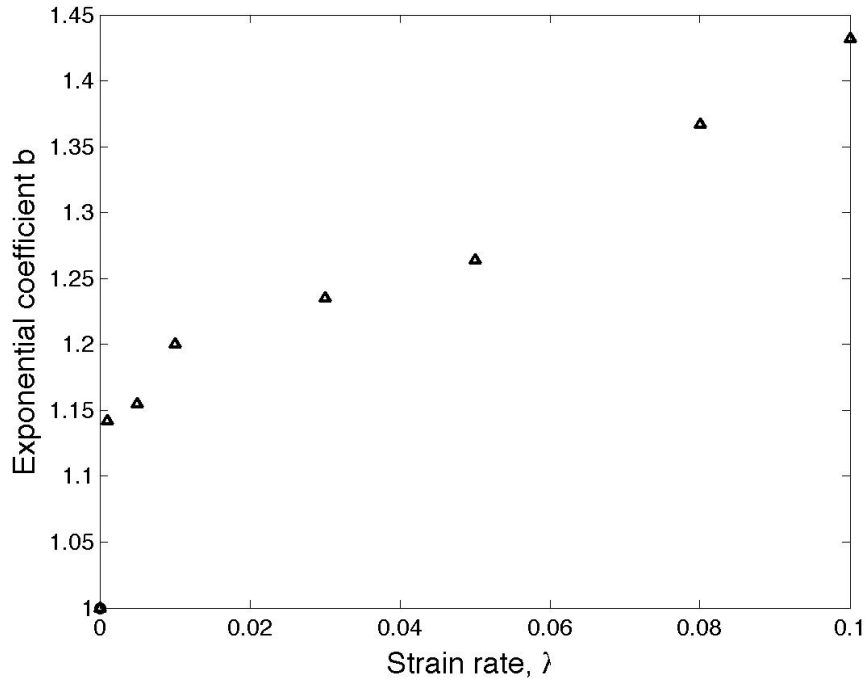
Figure 4.6. Plot of exponential coefficient b versus strain rate λ. Error bars are smaller than the size of the markers and thus are not shown (refer to table 4.2 for further information). Note how low strain rates approach the value of unity for zero strain rate as developed from Pantano and Pullin [42] (shown in a black dot).

Pantano and Pullin reported that it was analytically impossible to find a unique Λ for non-unity Lewis numbers; but, we determined the coefficients a and b numerically for a range of Lewis numbers. Note that a is highly dependent on Lewis number, even though b is not (it is indeed nearly constant within a strain rate, independent of Lewis number). As can be seen from Tables 4.3 and 4.4 and Figure 4.7, a does not increase linearly with the decrease in Lewis number but rather decreases logarithmically (as plotted on a log-log plot). The equations relating $\alpha = \log a$ to $\log Le$ are (as determined by Matlab's curve

Coefficient a for various strain rates and Lewis numbers			
Lewis number	$a_{\lambda=0.01}$	$a_{\lambda=0.05}$	$a_{\lambda=0.1}$
0.6	5.676	5.968	6.169
0.7	4.788	5.012	5.149
0.8	4.135	4.318	4.398
0.9	3.633	3.770	3.831
1.0	3.234	3.363	3.375
1.1	2.925	3.015	3.012
1.2	2.662	2.732	2.715
1.3	2.434	2.496	2.464
1.4	2.253	2.296	2.254
1.5	2.084	2.122	2.071

Table 4.3. Table of coefficient a for the exponential fit $v = ar_f^{-b}$ for flame velocity near the collapse for various Lewis numbers. Values were taken by fitting the data to the simulation results. Flames were started at $r = 16$ and allowed to collapse. Strain rates $\lambda = 0.01$, $\lambda = 0.05$ and $\lambda = 0.1$ are shown.

fitting algorithm):

$$\lambda = 0.1: \quad \alpha \;=\; -1.189 \log(Le) + 1.215 \quad \sigma^2 = 6.4 \times 10^{-4}$$

$$\lambda = 0.05: \quad \alpha \;=\; -1.127 \log(Le) + 1.211 \quad \sigma^2 = 4.0 \times 10^{-4}$$

$$\lambda = 0.01: \quad \alpha \;=\; -1.093 \log(Le) + 1.178 \quad \sigma^2 = 1.5 \times 10^{-3}$$

4.3.3. Critical Radius

To understand what influence the Lewis number has on the critical radius, we examine two different strain rates, $\lambda = 0.1$ and $\lambda = 0.05$. As discussed by Lu [3], for unity Lewis numbers, we expect the critical radius to decrease as strain rate decreases. Values for unity Lewis numbers correspond to results he reported. Moving beyond that, it is found

Table of $\alpha \pm 2\sigma_\alpha$ for various strain rates and Lewis numbers			
Lewis number	$\lambda = 0.01$	$\lambda = 0.05$	$\lambda = 0.1$
	$\alpha \pm 2\sigma_\alpha$	$\alpha \pm 2\sigma_\alpha$	$\alpha \pm 2\sigma_\alpha$
0.6	1.736 ± 0.002	1.786 ± 0.003	1.820 ± 0.004
0.7	1.566 ± 0.002	1.612 ± 0.002	1.639 ± 0.003
0.8	1.420 ± 0.002	1.463 ± 0.003	1.479 ± 0.002
0.9	1.290 ± 0.002	1.327 ± 0.002	1.343 ± 0.001
1.0	1.173 ± 0.002	1.213 ± 0.002	1.216 ± 0.002
1.1	1.073 ± 0.003	1.104 ± 0.002	1.103 ± 0.001
1.2	0.979 ± 0.001	1.001 ± 0.002	0.998 ± 0.001
1.3	0.890 ± 0.002	0.915 ± 0.002	0.902 ± 0.001
1.4	0.812 ± 0.001	0.831 ± 0.002	0.813 ± 0.001
1.5	0.734 ± 0.002	0.752 ± 0.002	0.728 ± 0.001

Table 4.4. Table of logarithmic coefficient $\alpha = \log(a)$ for the exponential fit $v = ar_f^{-b}$ for flame velocity near the collapse for various Lewis numbers. Values were taken by fitting the data to the simulation results. Flames were started at $r = 16$ and allowed to collapse. Strain rates $\lambda = 0.01$, $\lambda = 0.05$ and $\lambda = 0.1$ are shown, with $2\sigma_\alpha$ denoting the 95% confidence interval.

Table of $b \pm 2\sigma_\alpha$ for various strain rates and Lewis numbers			
Lewis number	$\lambda = 0.01$	$\lambda = 0.05$	$\lambda = 0.1$
	$b \pm 2\sigma_b$	$b \pm 2\sigma_b$	$b \pm 2\sigma_b$
0.6	1.210 ± 0.006	1.264 ± 0.006	1.432 ± 0.009
0.7	1.200 ± 0.007	1.261 ± 0.005	1.429 ± 0.007
0.8	1.207 ± 0.008	1.262 ± 0.006	1.430 ± 0.005
0.9	1.200 ± 0.007	1.255 ± 0.005	1.439 ± 0.003
1.0	1.200 ± 0.007	1.264 ± 0.006	1.432 ± 0.005
1.1	1.195 ± 0.008	1.258 ± 0.006	1.441 ± 0.004
1.2	1.169 ± 0.004	1.265 ± 0.006	1.440 ± 0.004
1.3	1.182 ± 0.004	1.256 ± 0.006	1.440 ± 0.003
1.4	1.165 ± 0.004	1.250 ± 0.006	1.439 ± 0.003
1.5	1.176 ± 0.005	1.242 ± 0.005	1.445 ± 0.002
average	1.190	1.257	1.436

Table 4.5. Table of exponential b for the exponential fit $v = ar_f^{-b}$ for flame velocity near the collapse for various Lewis numbers. Values were taken by fitting the data to the simulation results. Flames were started at $r = 16$ and allowed to collapse. Strain rates $\lambda = 0.01$, $\lambda = 0.05$ and $\lambda = 0.1$ are shown.
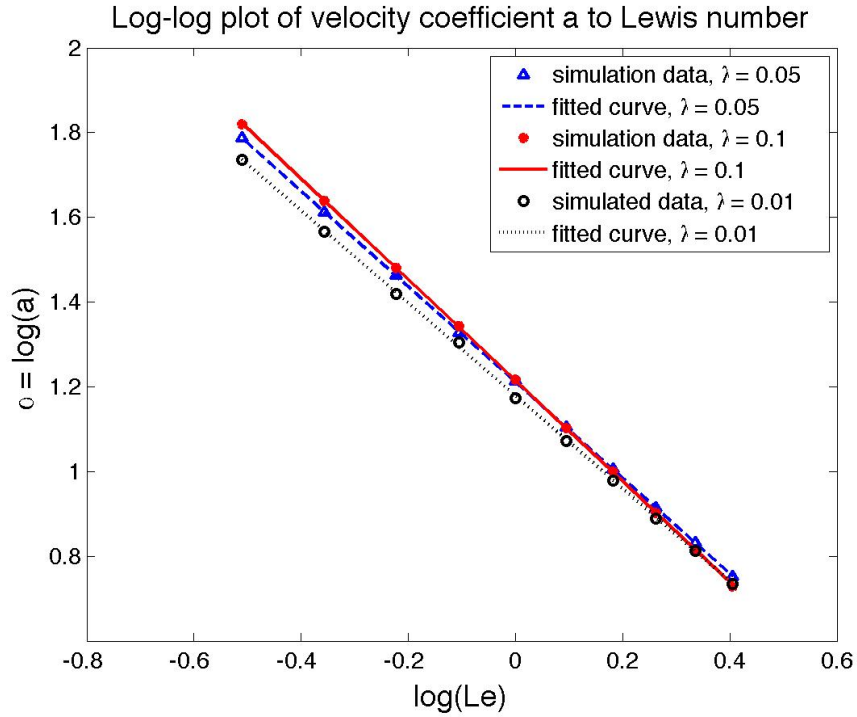
Figure 4.7. The relationship between the coefficient a in the curve fit to the collapsing radius ($v = ar_f^{-b}$) and the Lewis number is roughly linear in a log-log plot as can be seen from the data (points). Curve fit lines are given in the text for the different strain rates.

that the critical radius decreases with the increase in Lewis number. Specifically it is:

$$r_c = r_{c,Le=1.0}Le^{-0.5} \tag{4.38}$$

where the prefactor $r_{c,Le=1.0}$ would change to match the individual strain rate value of the $Le = 1.0$ critical radius (so when $\lambda = 0.1$, $r_{c,Le=1.0} = 3.35$ as shown in Figure 4.8). Figure 4.8 and Table 4.6 shows reported values for critical radii for various Lewis numbers. Interestingly, the values for critical radius scale with strain rate, for example at a given Lewis number, the critical radius at $\lambda = 0.05$ is 2.94 that at $\lambda = 0.1$. By finding the relationship between given values at unity Lewis numbers and knowing the relationships,

it is possible to extrapolate the values for any Lewis number. Using other strain rates (see Table 4.7) for both $Le = 0.6$ and $Le = 1.0$ the separations between the critical radii are shown to scale uniformly between strain rates.
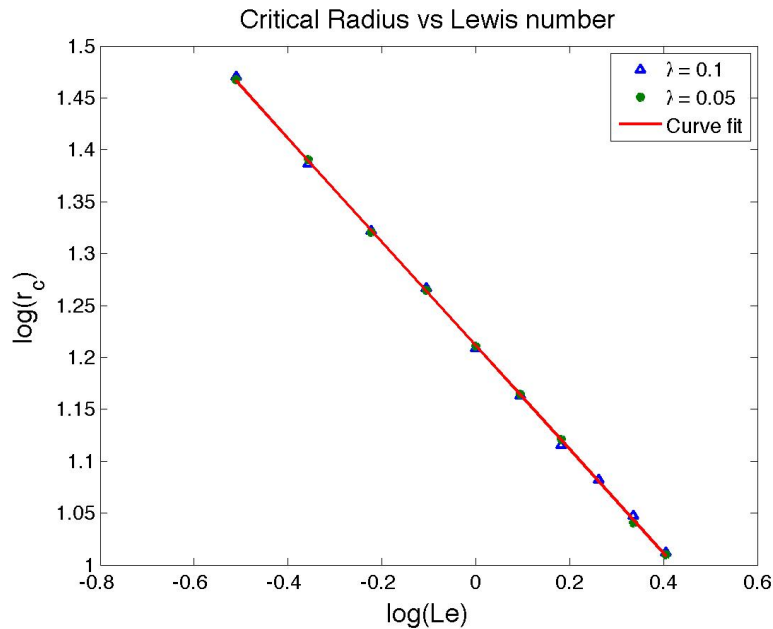
Figure 4.8. Critical radius vs. Lewis number (both non-dimensional) for $\lambda = 0.1$ and $\lambda = 0.05$ (note that $\lambda = 0.05$ has been scaled by a factor of 2.95 so as to lie on the $\lambda = 0.1$ curve). Here the curve fit is the line $r_c = 3.35 Le^{-0.5}$.

4.4. Conclusions

Through this study, we looked at the effect of Lewis number on the extinction of holes in planar flames. Examining general trends in the behavior of planar flames, we found that, as expected, temperature and reaction rate are tied to the Lewis number with both increasing as the Lewis number decreases. A correlation between the Lewis number and the critical radius was found showing that the critical radius is inversely proportional to the square root of the Lewis number. The flame velocity was also found to be strongly

Critical radii for different Lewis numbers		
Lewis number	$r_c(\lambda = 0.05)$	$r_c(\lambda = 0.1)$
0.6	12.80	4.35
0.7	11.85	4.00
0.8	11.05	3.75
0.9	10.45	3.55
1.0	9.9	3.35
1.1	9.45	3.20
1.2	9.05	3.05
1.3	8.75	2.95
1.4	8.35	2.85
1.5	8.10	2.75

Table 4.6. Critical radii for different strain rates and different Lewis numbers. Notice that the critical radii scales almost exactly the same between strain rates.

Critical radii for different strain rates			
λ	$r_c(Le = 0.6)$	$r_c(Le = 1.0)$	$r_{c(\lambda)}/r_{c(\lambda=0.1)}$
0.22	0.75	0.5	0.16
0.2	1.0	0.8	0.24
0.15	2.0	1.55	0.46
0.1	4.35	3.35	1.0
0.08	6.3	4.9	1.46
0.05	12.8	9.9	2.95

Table 4.7. Critical radii for different strain rates for Lewis numbers $Le = 0.6$ and $Le = 1.0$. The ratio of the radius at the given λ and that of $\lambda = 0.1$ is given in the right column.

dependent on Lewis number, and we developed a numerical relation showing that the prefactor a was dependent on the Lewis number while the exponent b was dependent on strain rate. A greater understanding of the Lewis number effects is important when trying to understand the different effects exhibited by different fuels. Through this study, we hope to extend the knowledge that is applicable only to unity Lewis number cases to

other situations, thus opening up a wider range of applicability for unity Lewis number simulations.

CHAPTER 5

Conclusion

While the study of laminar diffusion flames represent only a small subset of the rich and varied field of combustion phenomena, it has far reaching applications for the purpose of developing a fundamental understanding of systems from engines to kitchen ranges. Through these studies we have continued to develop the fundamentals essential to a fuller understanding of the complex processes behind the everyday phenomenon of fire.

The first part of my thesis involved the extinction of unstrained planar flames that were studied using a combination of experimental techniques and numerical simulation. The effect of burner configuration on extinction was explored, showing how the flame is steadier when oxidizer is flowing and how the extinction curves change when the fuel and oxidizer are switched. Comparisons between methane and propane were conducted showing that, in general, propane is a more stable system with extinction of propane occurring at lower fuel concentrations than methane. It was shown how flames are highly dependent on flow rate with various regions where burning is not possible. Along with this work, I presented a framework to examine instabilities in the methane/propane system, noting the different types of oscillations and when they occur. Since oscillations can greatly increase the concentration at which extinction occurs, it is essential to have a good understanding of these instabilities and when they occur to develop the most accurate concentration extinction curves. Also, I looked at numerical simulations and showed how simple one step chemistry models capture many of the same phenomena that the more

complex models exhibit, vindicating the use of simple chemistry in analytical work. These experiments and the numerical simulations used to model them create a bridge between observed flame behavior (in other burners and in other, non-laboratory settings) and analytical models where simple chemistry and flame structure are assumed.

In the second part of my thesis, numerical simulations of two dimensional, colliding planar flames were studied to determine the effects of the Lewis number on the collapse of flame holes. General observations of the effects of the Lewis number on planar flames including the effects of strain rate and Lewis number on temperature and reaction rate were presented showing how decreasing the Lewis number causes the flame to burn hotter and the flame to be thicker. On examining the speed of collapse of flame holes leading to re-ignition of quenched flame sheets, a scaling law for the dependence of edge propagation speed on hole radius was extracted from the data. I found that the "critical radius" (the maximum hole size that results in a re-ignition event) decreases with an increase in Lewis number and scales in a certain way with the strain rate. These studies add to the body of literature and increase the general understanding of the extinction or growth of flame holes.

Both of these studies examine important parameters necessary for the spreading or extinction of flames. By developing these fundamental models and connecting them to the systems we know how to model, we draw closer to being able to realistically model more complex systems such as turbulent combustion.

References

[1] S. Ghosal and L. Vervisch. Theoretical and numerical study of a symmetrical triple flame using the parabolic flame path approximation. *Journal of Fluid Mechanics*, 415:227–260, 2000.

[2] Z. Lu and S. Ghosal. A similarity solution describing the collision of two planar premixed flames. *Combustion Theory and Modelling*, 7:645–652, 2003.

[3] Z. Lu. *The Dynamics of Extinction and re-Ignition Processes on a Diffusion Flame Sheet.* PhD thesis, Northwestern University, 2003.

[4] G.F. Carrier, F.E. Fendell, W.B. Bush, and P.S. Feldman. Nonisenthalpic interaction of a planar premixed laminar flame with a parallel end wall. Technical report, Society of Automotive Engineers Paper 790245, 1979.

[5] G.F. Carrier, F.E. Fendell, and W.B. Bush. Interaction of a planar premixed flame with a parallel adiabatic end wall. *Combustion Science and Technology*, 20:195–297, 1979.

[6] W.B. Bush, F.E. Fendell, and S.F. Fink. Effect of boundary thermal constraint on planar premixed-flame/wall interaction. *Combustion Science and Technology*, 24:53–70, 1980.

[7] G.F Carrier, F.E. Fendell, and P.S. Feldman. Interaction of a planar laminar premixed flame with a perpendicular wall. Technical report, Society of Automotive Engineers Paper 800285, 1980.

[8] J.L. Duda and J.S. Vrentas. Perturbation solutions of diffusion-controlled moving boundary problems. *Chemical Engineering Science*, 24:461–470, 1969.

[9] F. Williams. *Combustion Theory, 2nd Ed.* Perseus Books Publishing, L.L.C., Reading, Massachusetts, 1985.

[10] Ya. B. Zeldovich, G.I. Barenblatt, V.B. Librovich, and G.M. Makhviladze. *The Mathematical Theory of Combustion and Explosions*. Consultants Bureau, New York, NY, 1985. Translated from the original Russian by D. H. McNeill.

[11] P. Clavin. Premixed combustion and gas dynamics. *Annual Review of Fluid Mechanics*, 26:321–52, 1994.

[12] J. Buckmaster, P. Clavin, A. Liñán, M. Matalon, N. Peters, G. Sivashinsky, and F.A. Williams. Combustion theory and modeling. *Proceedings of the Combustion Institute*, 30:1–19, 2005.

[13] E. Mallard and H. Le Chatelier. Recherches experimentales et theoriques sur la combustion des melanges gazeux explosifs. *Annales des mines, ou Recuell de memoires sur l'exploitation des mines, et sur les sciences qui s'y rapportant*, 4:274–295, 1883.

[14] F. Williams. *Combustion Theory*. Addison-Wesley Publishing Company, Reading, Pennsylvania, 1965.

[15] W.B. Bush and F.E. Fendell. Asymptotic analysis of laminar flame propagation for general lewis numbers. *Combustion Science and Technology*, 1:421–428, 1970.

[16] A.P. Kurkov and W. Mirsky. An analysis of the mechanism of flame extinction by a cold wall. *Twelfth Symposium (International) on Combustion*, pages 615–624, 1969.

[17] G.F. Carrier, F.E. Fendell, and P.S. Feldman. Nonisobaric flame propagation. *Dynamics and Modelling of Reactive Systems*, pages 333–351, 1980.

[18] D.E. Kooker. Numerical study of a confined premixed laminar flame: Oscillatory propagation and wall quenching. *Combustion and Flame*, 49:141–149, 1983.

[19] J. Buckmaster. The quenching of two-dimensional premixed flame. *Acta Astronautica*, 6:741–769, 1979.

[20] M Matalon, C. Cui, and J.K. Bechtold. Hydrodynamic theory of premixed flames: effects of stoichiometry, variable transport coefficients and arbitrary reaction orders. *Journal of Fluid Mechanics*, 487:179–210, 2003.

[21] C.L. Huang and Y.P. Shih. Perturbation solutions of planar diffusion-controlled moving boundary problems. *Int. Journal of Heat and Mass Transfer*, 18:689–695, 1975.

[22] L.J. Hartley and J.W. Dold. Flame propagation in a nonuniform mixture: Analysis of a propagating triple-flame. *Combustion Science and Technology*, 80:23–46, 1991.

[23] V. Nayagam, R. Balasubramaniam, and P.D. Ronney. Diffusion flame holes. *Combustion Theory and Modelling*, 3:727–742, 1999.

[24] G.R. Ruetsch, L. Vervisch, and A. Liñán. Effects of heat release on triple flames. *Physical Fluids*, 7(6):1447–1454, 1995.

[25] S.P. Burke and T.E.W. Schumann. Diffusion flames. *Industrial and Engineering Chemistry*, 20(10):998–1004, 1928.

[26] J.D. Buckmaster and G.S.S. Ludford. *Lectures of Mathematical Combustion.* Society for Industrial and Applied Mathematics, Philadelphia, Pennsylvania, 1983.

[27] Y.B. Zeldovich. On the theory of combustion of initially unmixed gases. *NACA Technical Memorandum 1296*, page 20, 1951.

[28] F. Fendell. Ignition and extinction in combustion of initially unmixed reactants. *Journal of Fluid Mechanics*, 21(2):281–303, 1965.

[29] A. Liñán. The asymptotic structure of counterflow diffusion flames for large activation energies. *Acta Astronautica*, 1:1007–1039, 1974.

[30] A. Liñán and A. Crespo. An asymptotic analysis of unsteady diffusion flames for large activation energies. *Combustion Science and Technology*, 14:95–117, 1976.

[31] J. Buckmaster. Edge-flames. *Journal of Engineering Mathematics*, 31:269–284, 1997.

[32] H. Phillips. Flame in a buoyant methane layer. *Tenth Symposioum (International) on Combustion*, pages 1277–1283, 1965.

[33] P.N. Kioni, B. Rogg, K.N.C. Bray, and A. Liñán. Flame speed in laminar mixing layers: The triple flame. *Combustion and Flame*, 95:276–290, 1993.

[34] J.W. Dold. Flame propagation in a nonuniform mixture: Analysis of a slowly varying triple flame. *Combustion and Flame*, 76:71–88, 1989.

[35] J. Buckmaster and M. Matalon. Anomalous lewis number effects in tribrachial flames. *Twenty-Second Symposium (International) on Combustion*, pages 1527–1535, 1988.

[36] T. Plessing, P. Terhoeven, N. Peters, and M.S. Mansour. An experimental and numerical study of a laminar triple flame. *Combustion and Flame*, 115:335–353, 1998.

[37] T. Echekki and J.H. Chen. Structure and propagation of methanol-air triple flames. *Combustion and Flame*, 114:231–245, 1998.

[38] J. Daou and A. Liñán. The role of unequal diffusivities in ignition and extinction fronts in strained mixing layers. *Combustion Theory and Modeling*, 2:449–477, 1998.

[39] M.L. Shay and P.D. Ronney. Nonpremixed edge flames in spatially varying straining flows. *Combustion and Flame*, 112:171–180, 1998.

[40] A.E. Potter, S. Heimel, and J. Butler. Apparent flame strength, a measure of maximum reaction rate in diffusion flames. In *18th International Symposium on Combustion*, pages 1027–103, Baltimore, MD, 1962. The Williams & Wilkins Company.

[41] J. Buckmaster and T.L. Jackson. Holes in flames, flame isolas, and flame edges. *Proceedings of the Combustion Institute*, 28:1957–1964, 2000.

[42] C. Pantano and D.I. Pullin. On the dynamics of the collapse of a diffusion-flame hole. *Journal of Fluid Mechanics*, 480:311–332, 2003.

[43] Z. Lu and S. Ghosal. Flame holes and flame disks on the surface of a diffusion flame. *Journal of Fluid Mechanics*, 513:287–307, 2004.

[44] R.J. Osborne, T.M. Brown, R.W. Pitz, M.A. Tanoff, and M.D. Smooke. Study of structure and emissions of partially premixed methane flames in laminar counterflow. *American Institute of Aeronautics and Astronautics*, 1996. Taken November 2, 2005 from: http://www.vuse.vanderbilt.edu/Research_Groups/Laser_Diagnostics/aiaa96.htm.

[45] K. Seshadri. Counterflow extinction of premixed and nonpremixed methanol and ethanol flames. *University of California Energy Institute*, 2005. Taken November 2, 2005 from: http://repositories.cdlib.org/ucei/basic/FSE007/.

[46] R. Seiser, K. Seshadri, E. Piskernik, and A. Liñán. Ignition in the viscous layer between counterflowing streams: Asymptotic theory with comparison to experiments. *Combustion and Flame*, 122:339–349, 2000.

[47] C.L. Chen and S.H. Sohrab. Simultaneous effects of fuel/oxidizer concentrations on the extinction of counterflow diffusion flames. *Combustion and Flame*, 86(4):383–393, 1991.

[48] B. Han, A.F. Ibarreta, C. Sung, and J.S. T'ien. Experimentally low-stretch gaseous diffusion flames in buoyancy-induced flowfields. *Proceedings of the Combustion Institute*, 30:527–535, 2005.

[49] S. Cheatham and M. Matalon. A general asymptotic theory of diffusion flames with application to cellular instability. *Journal of Fluid Mechanics*, 414:105–144, 2000.

[50] S. Kukuck and M. Matalon. The onset of oscillations in diffusion flames. *Institute of Physics Publishing*, 5:217–240, 2001.

[51] D. Lo Jacono, P. Papas, M. Matalon, and P.A. Monkewitz. An experimental realization of an unstrained planar diffusion flame. *Proceedings of the Combustion Institute*, 30:501–509, 2005.

[52] S.R. Biles, M.S. Jakulewicz, P. Papas, and D.G. Goodwin. Numerical simualations of planar unstrained diffusion flames in a porous plug counterdiffusion burner. *Western States Meeting of the U.S. Sections of the Combustion Institute*, 2005.

[53] M. Matalon and P. Papas. Characteristics of an unstrained diffusion flame in a porous plug counterdiffusion burner. *Proceedings of the Fourth Joint Meeting of the U.S. Sections of the Combustion Institute*, 2005.

[54] M. Matalon, G.S.S. Ludford, and J. Buckmaster. Diffusion flames in a chamber. *Acta Astronautica*, 6:943–959, 1979.

[55] D. Goodwin. *An open-source, extensible software suite for CVD process simulation*, volume PV 2003-08, chapter Chemical Vapor Deposition XVI and EUROCVD 14, pages 155–162. Editors M. Allendorf, F. Maury, F. Teyssandier, 2003. See also: http://www.cantera.org/.

[56] D. Lo Jacono. *Cell Formation in Diffusion Flames*. PhD thesis, Swiss Federal Institute of Technology Lausanne (EPFL), 2005.

[57] G.P. Smith, D.M. Golden, M. Frenklach, N.W. Moriarty, B. Eiteneer, M. Goldenberg, C.T. Bowman, R.K. Hanson, S. Song, W.C. Gardiner Jr, V.V. Lissianski, and Z. Qin. Grimech. http://www.me.berkeley.edu/gri_mech/.

[58] I.K. Puri and K. Seshadri. Extinction of diffusion flames burning diluted methane and diluted propane in diluted air. *Combustion and Flame*, 65:137–150, 1986.

[59] Y. Yahagi, S. Nakahara, K. Hamatsu, and M. Takeuchi. Effects of dilution and oxidizer preheating on extinction and structure of $ch_4 - o_2 - ar$ counterflowing diffusion flames, 2003. http://www.thp.mech.shibaura-it.ac.jp/.

[60] M. Matalon. Intrinsic flame instabilities in premixed and nonpremixed combustion. *Annual Review of Fluid Mechanics*, 39:163–191, 2007.

[61] D.A. Nield. Throughflow effects in the rayleigh-benard convective instability problem. *Journal of Fluid Mechanics*, 185:353–360, 1987.

[62] S. Duhr and D. Braun. Why molecules move along a temperature gradient. *Proceedings of the National Academy of Sciences*, 103(52):19678–19682, 26 December 2006.

[63] R. Ramanathan. *Introductory Econometrics with Applications.* South-Western, Mason, OH, 2002.

Curriculum Vitae

Jocelyn Elaine Renner

Contact Information

Northwestern University	*Cell:* (312) 339-2596
Dept. of Mechanical Engineering	*Work:* (847) 491-7470
2145 Sheridan Rd.	*E-mail:* jocelynrenner@gmail.com
Evanston, IL 60208, USA	*Website:* homepage.mac.com/jocelynrenner

Profile

Dissertation in the areas of combustion and fluid dynamics. Extensive experience in computer modeling, advanced mathematics, and experimental work. Held leadership roles on and off campus. Enjoy working in a team. Organizational experience including coordinating the technical conference at the Astronaut Scholars Annual Meeting and networking events for graduate students at Northwestern University. Background in Russian Studies and excellent communication skills. Teaching experience including lecturing, developing curricula and individual tutoring. Programming experience in MATLAB, FORTRAN, Mathematica, LaTeX, Excel, CANTERA and familiarity with Unix, Windows, and Macintosh OS X platforms.

<div align="center">EDUCATION</div>

Northwestern University, Evanston, Illinois USA

Ph.D. Mechanical Engineering, June 2008

- Dissertation Title: "Numerical and Experimental Studies of the Dynamics of Diffusion Flame Sheets"
- Advisors: Prof. Sandip Ghosal and Prof. Paul Papas
- Visiting Research Assistant at Colorado School of Mines, January 2006-August 2006.

University of Colorado, Boulder, Colorado USA

B.S., Applied Mathematics, May 2003

Minor, Astrophysics and Planetary Science

B.A., Russian Studies, May 2003

Study abroad at St. Petersburg State University, St. Petersburg, Russia, Summer 2001

Montrose High School, Montrose, Colorado, USA

<div align="center">PROFESSIONAL EXPERIENCE</div>

General Electric, Aviation Engineering, Cincinnati, Ohio USA

Engineer   **start date July 7, 2008**

<div align="center">HONORS AND AWARDS</div>

Honor Societies: Astronaut Scholars Honor Society, Tau Beta Pi, Phi Beta Kappa

Northwestern University: IGERT Complex Dynamics Fellow, 2003-2006, Cabell Fellow

2003-2004.

Colorado University: Outstanding Graduate for the College of Engineering, 2003. Colorado Engineering Council's Silver Medal Award Winner, 2003. Astronaut Scholar 2002-2003. Boettcher Scholar, 1998-2002. VIGRE Undergraduate Fellow 2001-2003.

Montrose High School: Valedictorian.

<div align="center">ACADEMIC RESEARCH</div>

Northwestern University, Evanston, Illinois USA   **September 2003-June 2008**

Graduate Research Assistant

- Analytic and numerical research in combustion studying planar flame deflagration
- Developed computer code to test new hypothesis
- Analysis of resulting data

Colorado School of Mines, Golden, Colorado USA   **January 2006-August 2006**

Visiting Research Assistant

- Experimental research into the extinction of laminar, planar flames using the PPCD burner
- Operated and maintained burner
- Conducted combustion experiments
- Computer modeling and comparative analysis of observed phenomena

University of Colorado, Boulder, Colorado USA   **September 2001-June 2003**

Undergraduate Research Assistant

- Investigation of the chaotic properties of rapidly rotating fluids

- Creating the analytical structure and mathematical model

- Coded computer simulation and ran numerical experiments

Teaching Experience

Teaching Assistant: Sophomore Fluid Dynamics course, Mechanical Engineering, NU

- Assistant lecturer

- Responsible for administrating and grading exams

- Developed new experimental procedure for fluids lab

- Organized and ran fluids lab course, including setting guidelines for laboratory expectations and grading labs.

- Conducted office hours, individualized education, and graded homework for course

- Generated solutions to homework, exams.

Teaching Assistant: Senior Transport Phenomena (Mass and Heat Transfer), Biomedical Engineering, NU

- Generated solutions to homework and gave input on problems. Posted solutions on web based software (Blackboard) as well as controlling posting of grades.

- Conducted office hours/review sessions for students

Teaching Assistant: Junior Manufacturing Automation course, Mechanical Engineering, NU

- Provided personal assistance through office hours

- Graded homework

Teaching Assistant: Graduate Dynamical Systems and Chaos, Applied Mathematics, NU

- Facilitated discussion sections on course material

Teaching Assistant: Calculus I, Applied Mathematics, CU

- Taught recitation section once a week

- Graded homework, exams

Undergraduate Student Teaching Assistant: Calculus Workshop, CU

- Assisted with design of curriculum and structure

- Led lab section

Tutor: Student Academic Services, CU

- Tutor for group and individuals in physics, math, and applied mathematics

Papers in preparation

S. Biles, M. Jakulewicz, P. Papas, and **J. Renner**. *Extinction Limits of Unstrained Planar Diffusion Flames.*

J. Renner and S. Ghosal. *Planar Flame Collision Dependence on Lewis Number.*

Conference Presentations

J. Renner and S. Ghosal. "An experimental and numerical study of the extinction of planar diffusion flames." Astronaut Scholars Honor Society Technical Conference, Cocoa Beach, FL, 2007.

J. Renner and P. Papas. "Influence of Mass Flux on Extinction of Unstrained Planar Diffusion Flames." NSF-IGERT Seminar, Evanston, IL, 2006.

J. Renner and P. Papas. "A numerical study of colliding diffusion flames." Astronaut Scholar Honor Society Technical Conference, Cocoa Beach, FL, 2006.

J. Renner and K. Julien. "Chaos: Modeling Dispersion Using Lyapunov Exponents." Astronaut Scholar Honor Society Technical Conference, Cocoa Beach, FL, 2003.

Leadership and Community Involvement

Community Leadership and Service

McCormick Graduate Leadership Council (NU)

- Organize networking events for graduate students including coordinating event space, managing food procurement, and promotion of events.
- Responsible for procurement, McCormick Art Fair 2008.

Mechanical Engineering Graduate Student Society (MEGSS) (NU)

- Treasurer (2005-2006)

NSF IGERT Dynamics of Complex Systems in Science and Engineering at Northwestern University

Member of PEO, a philanthropic women's organization, Chapter GC, Illinois

- Recording Secretary 2006-2007
- President 2007-2008
- Coordinated the processing of scholarship applicants

Lay speaker and choir member for local church

Society Memberships:

Society for Industrial and Applied Mathematics (SIAM)

The Combustion Institute

American Physical Society (APS)